Development of Design Wind Speed Maps for the Caribbean for Application with the Wind Load Provisions of ASCE 7

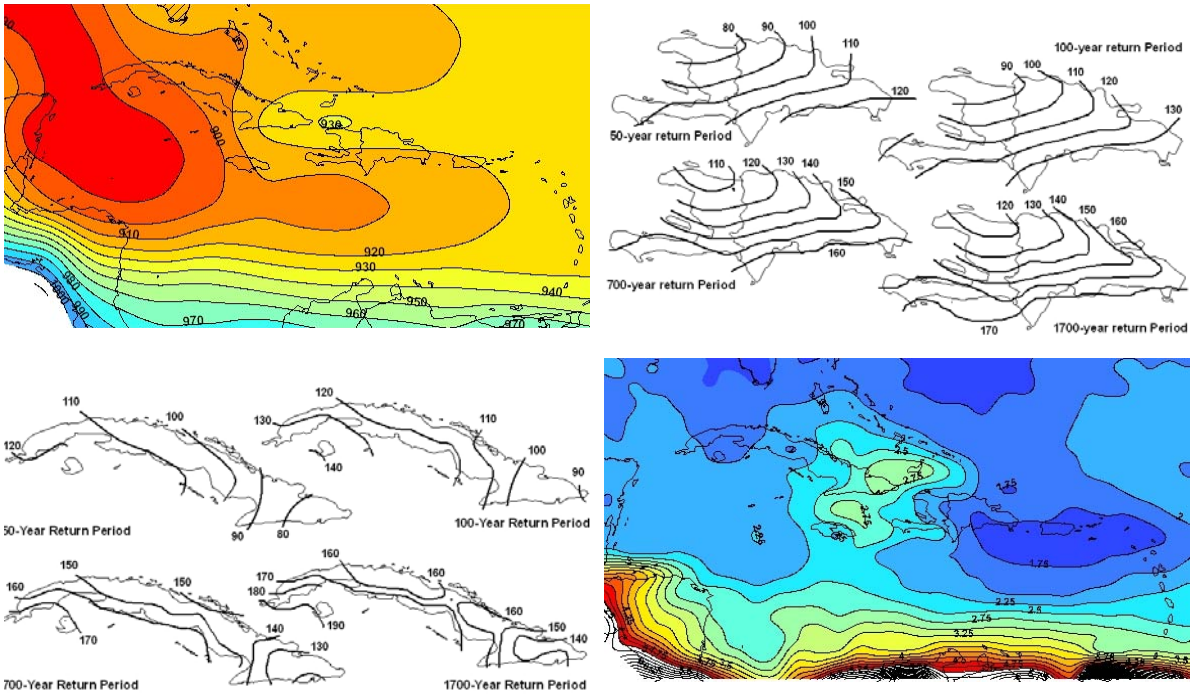

Area on Emergency Preparedness and Disaster Relief Coordination
525 23rd Street, N.W.
Washington, DC 20037-2875

This study was prepared by:

P. J. Vickery and D. Wadhera
Applied Research Associates, Inc.
8540 Colonnade Centre Drive, Suite 307
Raleigh NC 27615
ARA Report 18108-1

Under a special grant from the Office of Foreign Disaster Assistance of the United States Agency for International Development (OFDA/USAID).

The study has been made possible through the financial support of the Division of Humanitarian Assistance, Peace and Security of the Canadian International Development Agency (HAPS/CIDA) and the Office of Foreign Disaster Assistance of the United States Agency for International Development (OFDA/USAID).

1. INTRODUCTION

The objective of this study is to develop estimates of wind speeds as a function of return period for locations in the Caribbean Basin that can be used in conjunction with the design wind provisions used in the US wind loading standards that reference ASCE 7-98 and later. Maps of hurricane induced wind speeds are developed using a peer reviewed hurricane simulation model as described in Vickery et al. (2000a, 2000b, 2006, 2008a, 2008b), and Vickery and Wadhera (2008). The hurricane simulation model used here is an updated version of that described in Vickery et al. (2000a, 2000b) which was used to produce the design wind speeds used in ASCE 7-98 through to the ASCE 7-05, the current version.

Section 2 of the report describes the simulation methodology and model validation results, and section 3 presents the wind speed results and provides some guidance as to how these wind speeds should be used in conjunction with the requirements of the ASCE 7. A summary is presented in section 4.

2. METHODOLOGY

The hurricane simulation approach used to define the hurricane hazard in the Caribbean consists of two major components. The first component comprises a hurricane track model that reproduces the frequency and geometric characteristics of hurricane tracks as well as the variation of hurricane size and intensity as they move along the tracks. The second portion of the model is the hurricane wind field model, where given key hurricane parameters at any point in time from the track model, the wind field model provides estimates of the wind speed and wind direction at an arbitrary position. The meteorological inputs to the wind field model include the central pressure difference, Δp, translation speed, c, radius to maximum winds (*RMW*) and the Holland B parameter. (For computing Δp, the far field pressure is taken as 1013 mbar, and thus Δp is defined as 1013 minus the central pressure, p_c.) The geometric inputs include storm position, heading and the location of the site where wind speeds are required. The following sections describe the verification of the track model for the Caribbean and a summary of the wind field model is also presented.

2.1 Track and Intensity Modelling

The hurricane track and intensity simulation methodology used to define the hurricane hazard in the Caribbean follows that described in Vickery et al. (2000, 2008), but the coefficients used in the statistical models have been calibrated to model the variation in storm characteristics throughout the Caribbean basin.

Track and Relative Intensity Modelling The over water hurricane track simulation is performed in two steps. In the first step, the hurricane position at any point in time is modelled using the approach given in Vickery et al. (2000a). In the second step, the relative intensity, I, of the hurricane is modelled using a modified version of the approach given in Vickery et al. (2000a) as described in Vickery et al. (2008a) The relative intensity is then used to compute the central pressure, as described in Vickery et al (2000a). Then, using this central pressure, the *RMW* and B are computed as described in Vickery and Wadhera (2008) and Vickery et al (2008a). A simple one dimensional ocean mixing model, described in Emanuel et al. (2006), is used to simulate the effect of ocean feedback on the relative intensity calculations. The ocean mixing model returns an estimate of a mixed layer depth which is used to compute the reduction in sea surface temperature caused by the passage of a hurricane. This reduced sea surface temperature is used to convert historical pressures to relative intensity values. The historical relative intensity values are then used to develop regional statistical models of the form of Equation 2-1, where the relative intensity at any time is modelled as a function of relative intensity at last three steps and the scaled vertical wind shear, V_s, (DeMaria and Kaplan, 1999).

$$\ln(I_{i+1}) = c_1 \ln(I_i) + c_2 \ln(I_{i-1}) + c_3 \ln(I_{i-2}) + c_4 V_s + \varepsilon \qquad (2\text{-}1)$$

where c_1, c_2, etc. are constants that vary with region in the Atlantic Basin, and ε is a random error term. If a storm crosses land, the central pressure is computed using a

filling model, where the central pressure *t* hours after landfall is dependent on the storm pressure at the time of landfall and the number of hours that the storm has been over land.

Storm Filling Unlike hurricanes making landfall along the US mainland coastline, in the case of the Caribbean there is insufficient historical data available to develop island specific hurricane weakening (or filling) models for hurricanes passing over islands in the Caribbean. The limited data available to develop a statically based hurricane filling model is primarily a result of the 6 hour temporal resolution associated with HURDAT data, coupled with the fact that there is no additional information on landfall and exit pressures for those storms that do cross islands. In the storm intensity model described herein, we found that the filling model described in Vickery (2005) originally developed for use with hurricanes making landfall along the New England coast results in a variation in storm intensity statistics across islands that best matched the historical data. The use of the New England coast filling model provided the best model-data comparisons of storm central pressure statistics, with the other models described in Vickery (2005) yielding overestimates of storm intensity (as defined by central pressure) for regions on the lee sides of larger landmasses (Hispaniola, Cuba, Yucatan Peninsula). This overestimate of intensity indicates that storms crossing these land masses fill more rapidly than is predicted using any of the other (Gulf of Mexico, Florida Peninsula or Atlantic Coast) filling models given in Vickery (2005).

2.1.1 Model Validation

In the model validation/calibration process we compared the statistics of storm heading, translation speed, *c*, distance of closest approach, central pressure and annual occurrence rates for modelled and historical storms passing within 250 km of a grid-point. The distance of closest approach, $d_{\min}$, is defined as positive if a storm passes to the left of a site (centre of the circle) and negative if the storm passes to the right. Storm heading, θ, is measured clockwise from true north, such that a heading of 0 degrees represents a storm heading due north, 90 degrees represents a storm heading due east and -90 degrees represents a storm moving towards the west. The annual storm occurrence rate, λ, is defined as the total number of storms that enter the circle during the period of record divided by the record length. All storms in the HURDAT data base are used in the development of the model, not just those that reach hurricane intensity. The parameters *c*, $d_{\min}$, and θ are all computed at the point of closest approach to the centre of the circle. The central pressure values used in the validation procedure are the minimum values measured or modelled at any time while the storm is in the circle. For this study, we perform the comparisons using overlapping 250 km radius circles centred on a 2 degree grid spanning from 10^{o} N to 26^{o} N, and 59^{o} W to 91^{o} W. Figure 2-1 shows the location of the 140 grid points and the extent of the 250 km radius circles used in the validation/calibration process.

The HURDAT data set used in the model validation includes all tropical cyclones encompassing the period 1900 through 2007. However, central pressure data is only available for about 40% of the data points in the Caribbean. As noted in Georgiou et al. (1983), Georgiou (1985), and Vickery et al. (1995), we assume that the missing central

pressure data belong to a population having the same statistical distribution (given the occurrence of a storm) as the measured data. We also assume that prior to approximately 1970 (after which time central pressure data is available for nearly all storms) that there is no bias in the reporting of the sparse central pressure data given in HURDAT. Furthermore, unlike the case of the mainland US data, there is no supplemental data base of central pressures at the time of land fall extending back to 1900. The landfall database (Blake et al. 2007) provides the central pressure at the time of landfall for almost all hurricanes that made landfall along the US coastline since 1900. Thus, even though the pressure data within HURDAT is sparse for pre-1970 storms, the landfall data base extends back over 100 years is considered quite reliable. This additional landfall data enables statistical models for US landfall hurricanes to be validated with data having an effective period of record in excess of 100 years. In the case of the Caribbean, the effective period of record for data containing information on storm intensity as defined by central pressure is in the neighborhood of only 40 to 50 years.

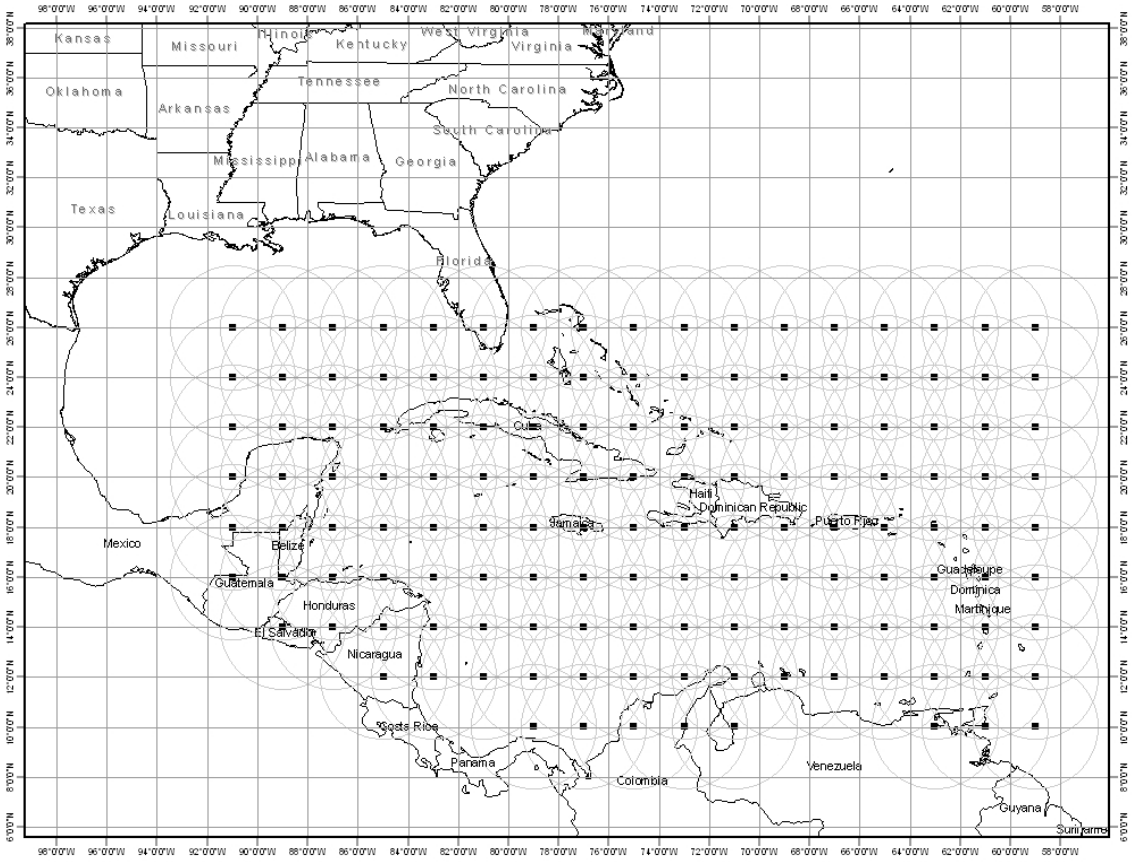

Figure 2.1 Locations of simulation circle centres showing extent of 250 km sample circles

In order to verify the ability of the model to reproduce the characteristics of historical storms we perform statistical tests comparing the characteristics of model and observed hurricane parameters. The statistical tests include *t*-tests for equivalence of means, *F*-tests for equivalence of variance and the Kolmogorov-Smirnov (*K-S*) tests for equivalence of the Cumulative Distribution Functions (CDF). In the case of central pressures we also used a statistical test method described in James and Mason (2005) for

testing equivalence of the modelled and observed central pressure conditional distributions of pressure, and as a function of annual exceedance probability. No consideration is given to the measurement errors inherent in the HURDAT data in the computation of translation speed, heading, central pressure, etc., in any of the statistical tests.

Figures 2-2 and 2-3 indicate the centres of the circles where the *t* and *F*-tests for modelled and observed parameters fail equivalence testing. Table 2-1 summarizes the failure rate for each of the parameters by test type and variable. As noted in Table 2-1, at a large number of locations (~16%), the modelled and observed storm heading data fail the *F*-test for equivalence of variances, and as a result, these data were examined in more detail through both visual comparisons of the cumulative distribution functions and by performing additional formal statistical tests (K-S). Appendix A presents graphical comparisons of the modelled and observed CDF for each variable. Figure 2-4 presents graphical comparisons of the CDFs for all locations where the *F*-test and K-S tests for storm heading failed.

Table 2-1. Percent of locations failing the indicated statistical equivalence tests at the 95% confidence level. Number of points failing equivalency is given in parentheses.

Variable	*t*-test	*F*-test	*K-S* test
Occurrence Rate	0.0% (0)	N/A	
d_{min}	6.4% (9)	2.1% (3)	
Translation speed	5.7% (8)	6.4% (9)	5.7% (8)
Heading	3.6% (5)	15.7% (22)	11.4% (16)
Central Pressure	0	4.2% (6)	5.0% (7)

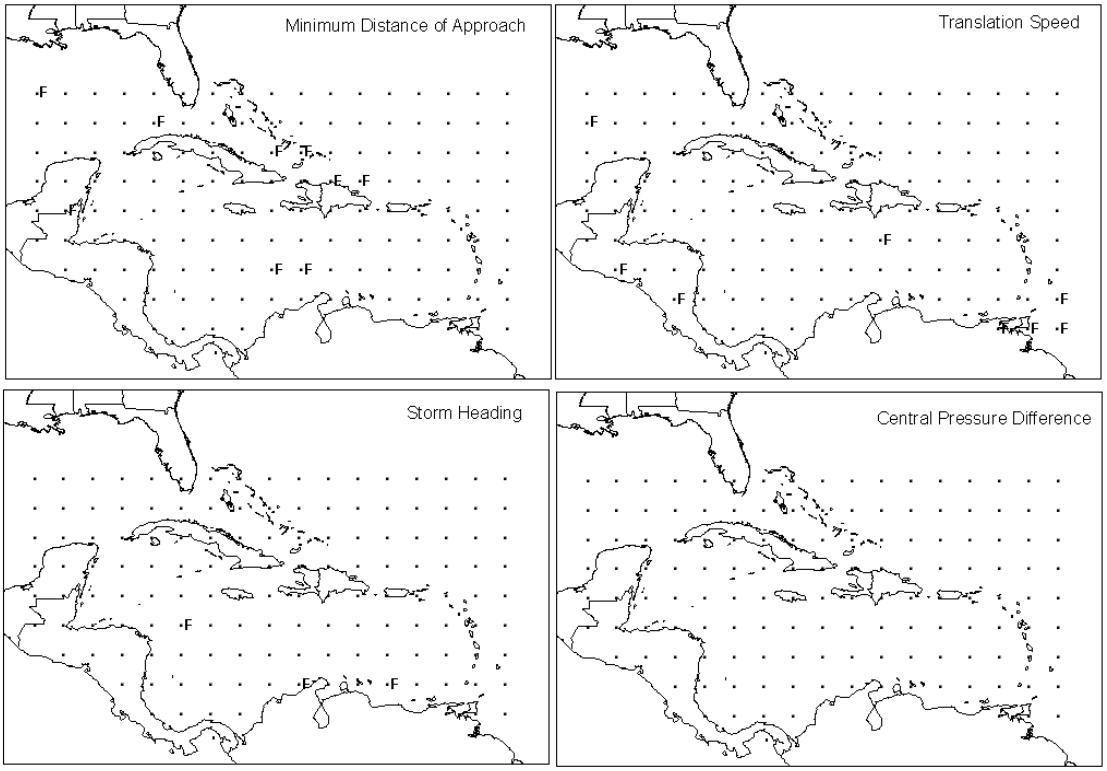

Figure 2-2 Locations where t-tests fail at the 95% confidence level.

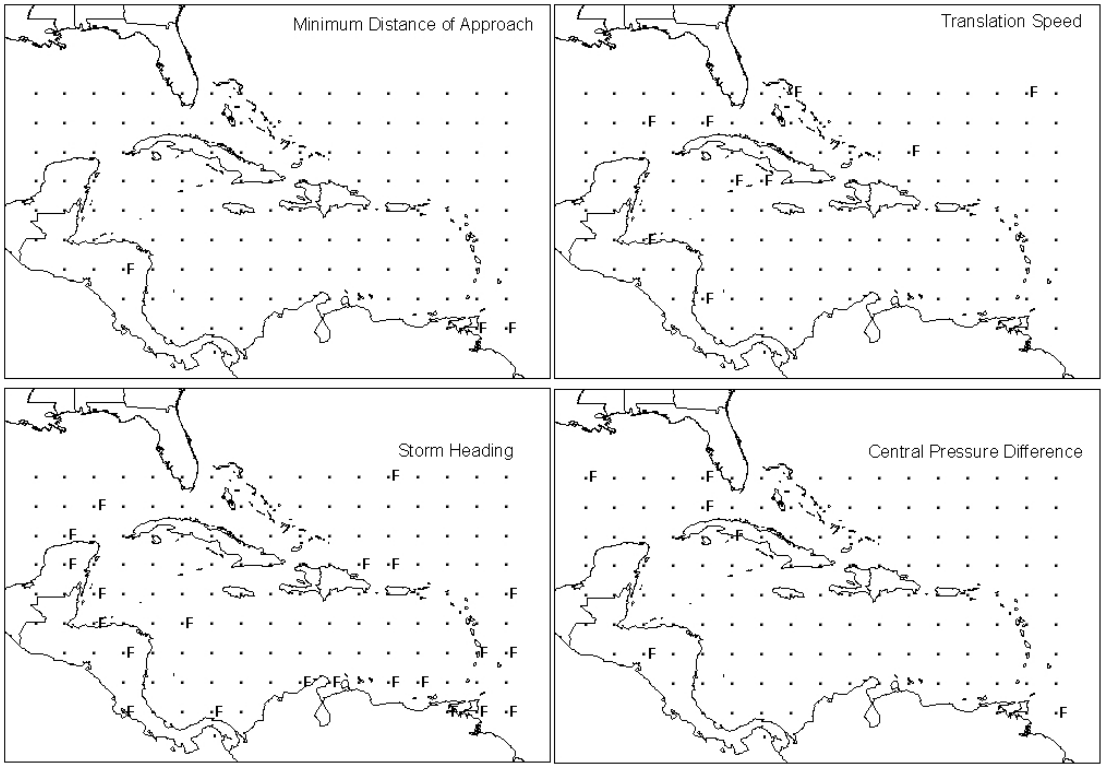

Figure 2-3 Locations where F-tests fail at the 95% confidence level.

In the case of translation speed and heading, more than one statistical test (*t*, *F* or *K-S*) is failed at the same location in only 3.6% of the cases.

For those locations where the model fails the *F*-test for heading equivalence, a visual comparison of the modelled and observed CDF data given in Appendix A and Figure 2-4 indicates that overall the model reproduces the observed heading data very well, and the variance of the observed data is strongly dependent on a few outliers. In most cases, these outliers are associated with the infrequent occurrence of one, or at most two, storms heading in an easterly direction in the southern portion of the Caribbean. In the southern portion of the Caribbean, the model produces eastward moving storms, but the occurrence of these eastward moving storms is distributed over a wider range of sample/validation circles than the historical storms, yielding both overestimates and underestimates of the variance, depending upon which circle the few historical storms happen to pass through. For those locations that fail the *F*-tests for heading equivalence in the Western Caribbean the model results tend to have a broader distribution.

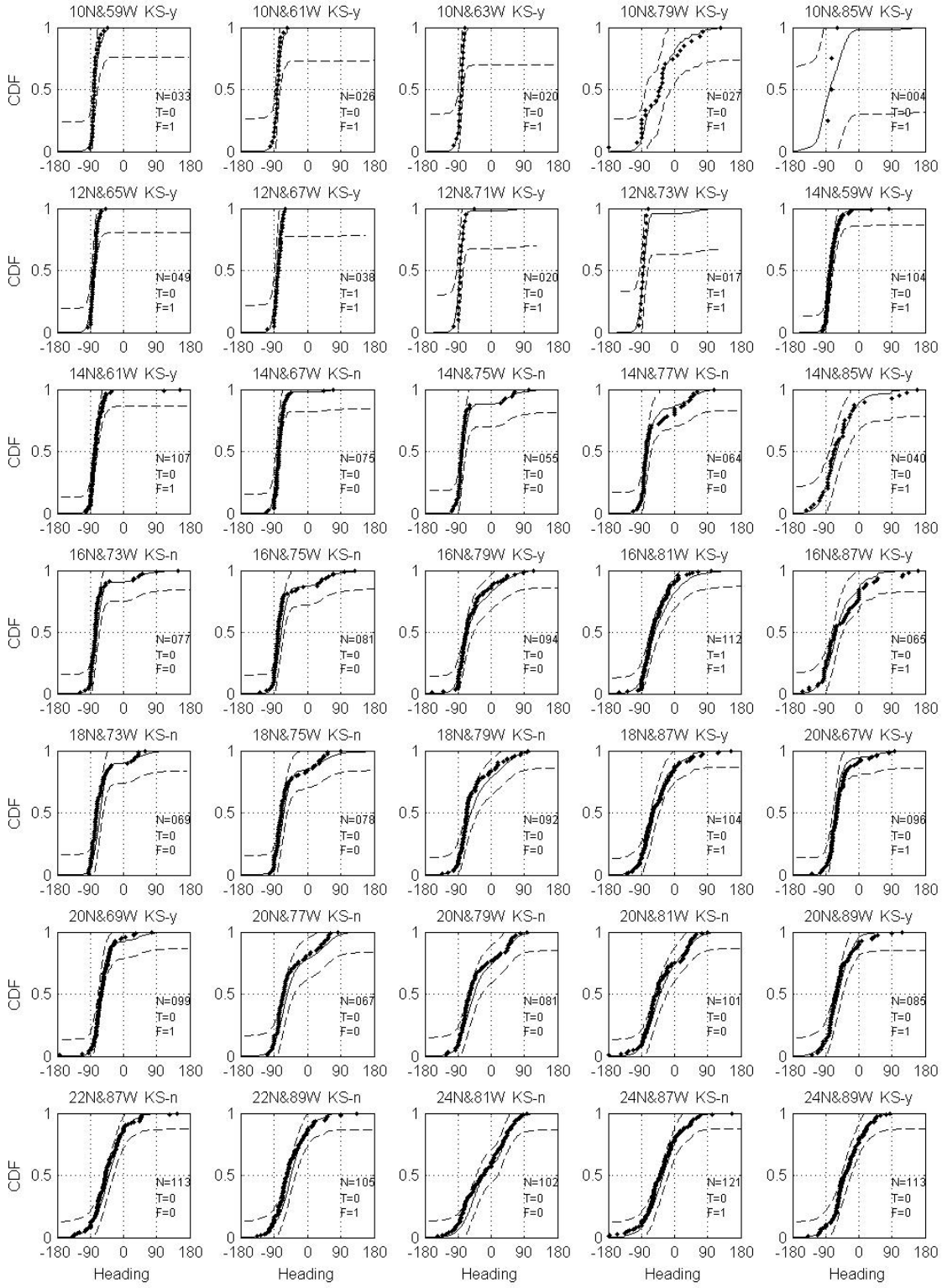

Figure 2-4 Comparisons of modelled and observed CDF's for locations failing the *F*-test for Equivalence of Variance. F=1 indicates failure of *F*-test, T=1 indicates failure of the t-test, KS-n indicates failure of the KS test. Dashed lines represent the KS test limit plotted as an offset from the model CDF.

Figure 2-5 presents a comparison of modelled and observed central pressures plotted versus return period for 35 locations in the Caribbean. The 35 locations follow along the Lesser and Greater Antilles, the Bahamas, Aruba, and coastal Central America, and thus encompass most of the populated region of the Caribbean. The observed central pressures plotted vs. return period were computed assuming the N_p pressure data points obtained from a total of N tropical cyclones that pass through the circle are representative of the full population of N storms. With this assumption, the CDF for the conditional distribution for storm central pressure is computed, where each pressure has a probability of $1/(N_p+1)$. The return period associated with a given central pressure is obtained from

$$1/RP = 1 - \exp[-\lambda P(p_c < P_c)] \tag{2-2}$$

where $P(p_c < P_c)$ is the probability that the central pressure p_c is less than P_c given the occurrence of any one storm, and λ is the annual occurrence rate defined as N/N_Y where N_Y is the number of years in the historical record, taken here as 108 years (1900 through 2007). The model estimates of central pressure versus return period are computed using Equation 2-2, where λ is simply the number of storms that enter the circle during the 100,000 simulated years divided by 100,000 and the probability distribution for central pressure is obtained by rank ordering the simulated central pressures.

In addition to the mean model estimates of pressure vs. return period, each of the plots given in Figure 2-5 also presents the 2.5^{th} and 97.5^{th} percentile (95% confidence range) values of central pressures derived by sampling N_p different values of central pressure from the simulated storm set and computing the CDF and then the pressure RP curve using the model value of λ. This process was repeated 1000 times, yielding 1,000 different *RP* curves based on sampling N_p pressures randomly from the simulated storm set. The 1,000 different *RP* curves are then used to define the 95% confidence range for the mean pressure *RP* curves. Testing for equivalence of empirical distributions using this re-sampling approach is presented in James and Mason (2005), who indicate that for sample sizes of the order of 20, the method is as powerful as either the Cramer-von Mises or Anderson-Darling tests for equivalence. Of the 35 p_c-*RP* curves given in Figure 2-5, two cases fail the empirical distribution equivalence testing method, as indicated by the notation *JM=n* at the top of the plot. Failure is defined as one or more observed values falling outside the bounds of the 2.5^{th} and 97.5^{th} percentile curves. In our testing, we only include tropical cyclones with central pressures less than 990 mbar. The equivalence testing of the p_c-*RP* curves yields a comparison that includes the combined effects of the modelling of both the central pressures and the frequency of occurrence of the storms.

Figure 2-6 presents a qualitative comparison of the modelled and observed extreme central pressures in the Caribbean. The observed values are presented as contours of the minimum observed central pressure *anywhere* within 250 km of the indicated point. The modelled values represent the minimum pressures *anywhere* within 250 km of the indicated point, likely to be exceeded, on average, once every 50 years

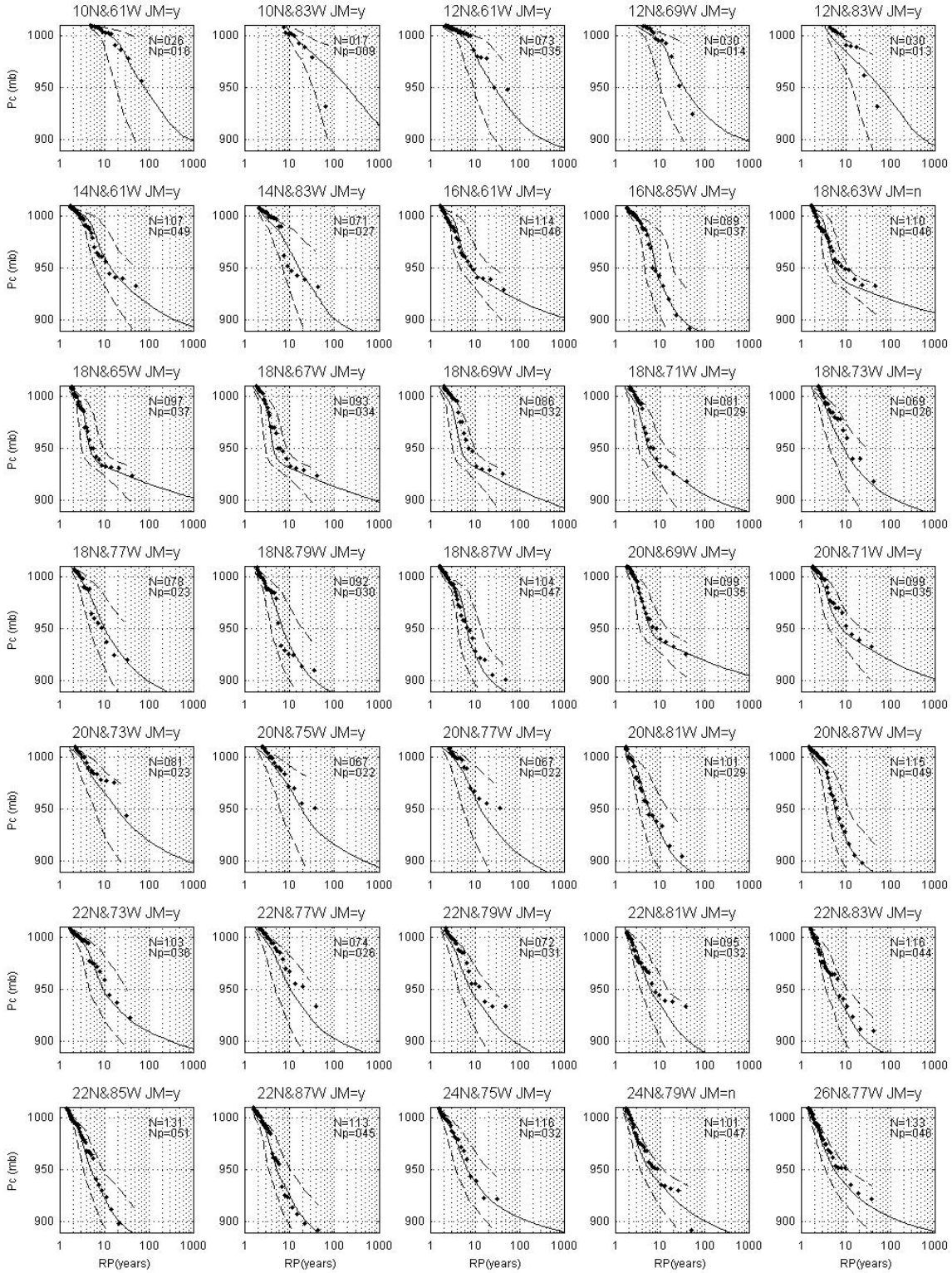

Figure 2-5 Modelled and observed central pressures vs. return period for points located near populated islands in the Caribbean. N=total number of tropical cyclones, N_p=number of tropical cyclones with pressure measurements. JM = n indicates failure of the empirical distribution equivalence test proposed by James and Mason (2005).

The effective period of record for the historical data is not known since there are relatively few pressure measurements in the Caribbean basin prior to the ~1970's, and at any given location the minimum pressure represents the minimum value obtained during a period varying from perhaps 30 or 40 years long to, at most, about 100 years long. Qualitatively, the comparison shows that the model reproduces the region of intense hurricanes passing to the south of the Greater Antilles and up through the Yucatan Channel. The magnitude of the modelled 50 year return period pressures are similar to the observed values, but reflect the smoothing expected for predicted mean values rather than single point observations from a ~50 year record. The increase in hurricane central pressure near the south east end of Cuba is not as pronounced in the model estimates suggesting that south-east Cuba has been lucky during the short period of record, or the model may be overestimating the intensity of hurricanes in this area.

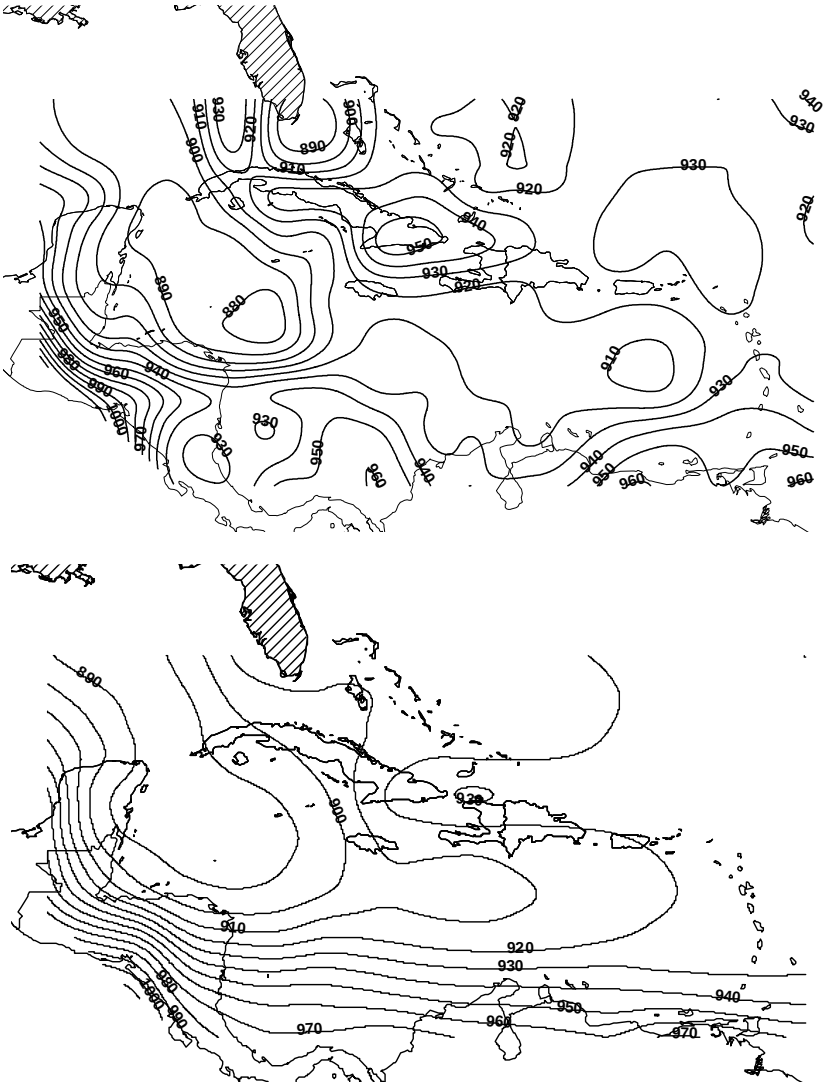

Figure 2-6 Contour plots of observed (upper plot) minimum central pressures (mbar) and modelled 50 year return period pressures (lower plot). Contours represent the minimum pressure *anywhere* within 250 km of a point.

2.2 Wind Modelling

The hurricane wind field model used here is described in detail in Vickery et al. (2008b). A brief overview of the hurricane wind field model is given below.

The model consists of two basic components, namely a 2-D finite difference solution for the equations of motion for a 2-D slab model used to describe the horizontal structure of the hurricane boundary layer, and a 1-D boundary layer model to describe the variation of the horizontal wind speed with height. The main reason for using a 2-D numerical model is that it provides a means to take into account the effect of surface friction on wind field asymmetries, as well as enabling the model to predict super gradient winds, and also to model the enhanced inflow caused by surface friction, particularly at the sea-land interface. The inputs to the slab model include Δp, the Holland B parameter, RMW and translation speed.

The results from the 2-D slab model are coupled with a boundary layer model that reproduces the variation of the horizontal wind with height. This model has been developed using a combination of experimental and theoretical analyses. The experimental data consists of the analysis of dropsonde data collected in hurricanes during the period from 1997 through 2003. As described in Vickery et al. (2008b), the variation of the mean horizontal wind speed, $U(z)$ with height z, in the hurricane boundary layer can be modelled using:

$$U(z) = \frac{u_*}{k}\left[\ln(\frac{z}{z_o}) - 0.4(\frac{z}{H^*})^2\right] \tag{2-3}$$

where k is the von-Karman coefficient having a value of 0.4, u_* is the friction velocity, z_{oo} is the surface roughness length, and H^* is a boundary layer height parameter that decreases with increasing inertial stability according to:

$$H^* = 343.7 + 0.260 / I \tag{2-4}$$

where the inertial stability parameter, I, is defined as:

$$I = \sqrt{(f + \frac{2V}{r})(f + \frac{V}{r} + \frac{\partial V}{\partial r})} \tag{2-5}$$

V is the azimuthally averaged tangential gradient wind speed, f is the Coriolis parameter and r is the radial distance from the centre of the storm. Over the ocean, the surface roughness, z_o, is estimated from

$$z_0 = 10\exp(-k / \sqrt{C_{d_{10}}}) \tag{2-6}$$

where $C_{d_{10}}$ is the sea surface drag coefficient computed from:

$$C_{d_{10}} = (0.49 + 0.065U(10))10^{-3}; \quad C_{d_{10}} \le C_{d_{\max}} \tag{2-7a}$$

$$C_{d_{\max}} = (0.0881r + 17.66)10^{-4}; \quad 0.0019 \le C_{d_{\max}} \le 0.0025 \tag{2-7b}$$

where r is the radial distance from the storm centre (km), but r is constrained to have a minimum value equal to the *RMW*. The limiting value of the sea surface drag coefficient used in the wind field model differs from that used in Vickery et al. (2000b) and Vickery and Skerlj (2000), where C_d continues to increase with wind speed. The effect of limiting C_d is to place a limit on the aerodynamic roughness of the ocean, and thus unlike the wind field model described in Vickery et al. (2000b), the model used here does not yield aerodynamic roughness values over the open ocean that approach those of open terrain values in high winds. This limiting, or capping, of the sea surface drag coefficient is discussed further in Powell et al. (2003) and Donelan et al. (2004). The consequences of the reduced, or limited, drag coefficient with respect to the calculation of wind loads using ASCE 7 is discussed in Simiu et al. (2007), where it is indicated that the use of exposure D for the design of structures near the hurricane coastline is appropriate.

Figure 2-7 presents examples of the modelled and observed variation of wind speed with height. The only input to the velocity profile model is the wind speed at gradient (or jet) height, computed from the 2-D slab model for the hurricane.

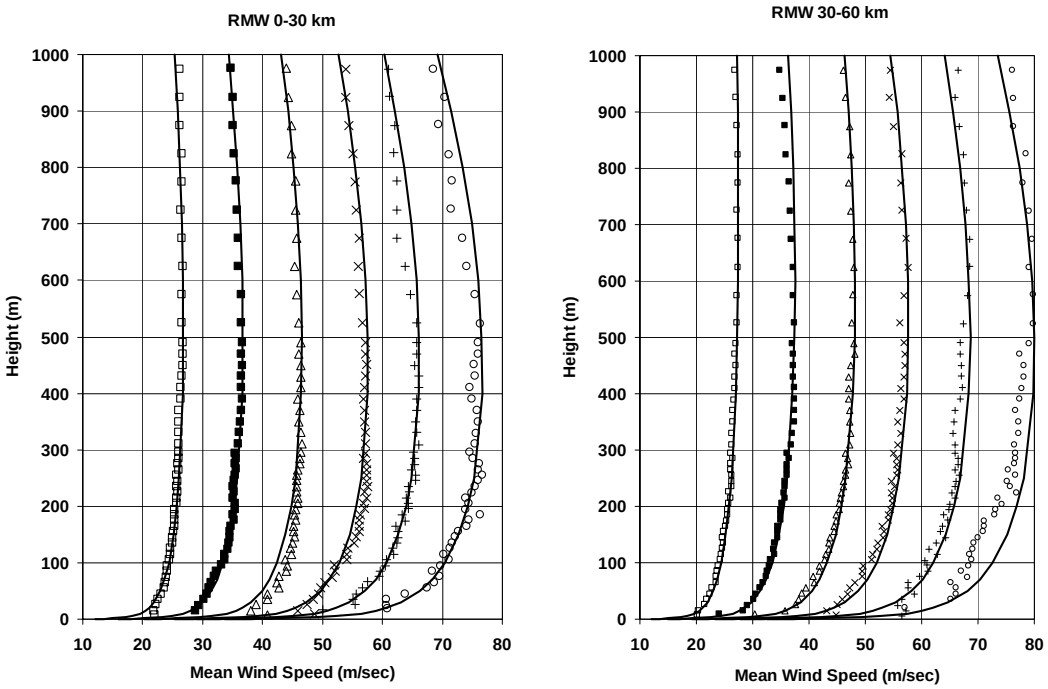

Figure 2-7. Modelled and observed hurricane mean vertical profiles of horizontal wind speed over the open ocean for a range of mean wind speeds

As the wind moves from the sea to the land, the value of the maximum wind speed at a given height in the new rougher terrain approaches the fully transitioned value, representative of the new rougher terrain, asymptotically over some fetch distance, *F*. For

modelling the transition from sea to land, the ESDU (1982) boundary layer transition model is used, but the limiting fetch distance of about 100 km used in ESDU (1982) is reduced to 20 km. This smaller fetch distance is consistent with the lower boundary layer heights associated with tropical cyclones (~600 m) compared to the larger values (~3000 m) used in ESDU for winds not produced by tropical cyclones. Figure 2-8 presents a plot showing the percentage the wind speed has transitioned (reduced) from the overwater values to the overland values as a function of distance from the coast. Note that at a distance of about 1 km from the coast, the peak gust wind speed has transitioned to about 70% of the fully reduced value. In a typical strong hurricane, the surface roughness, z_o will be about 0.003m, and the open terrain value is 0.03m. From ESDU (1982) the full transitioned values of the peak 3 second gust and hourly mean wind speeds are about 89% and 83% of the marine winds, respectively.

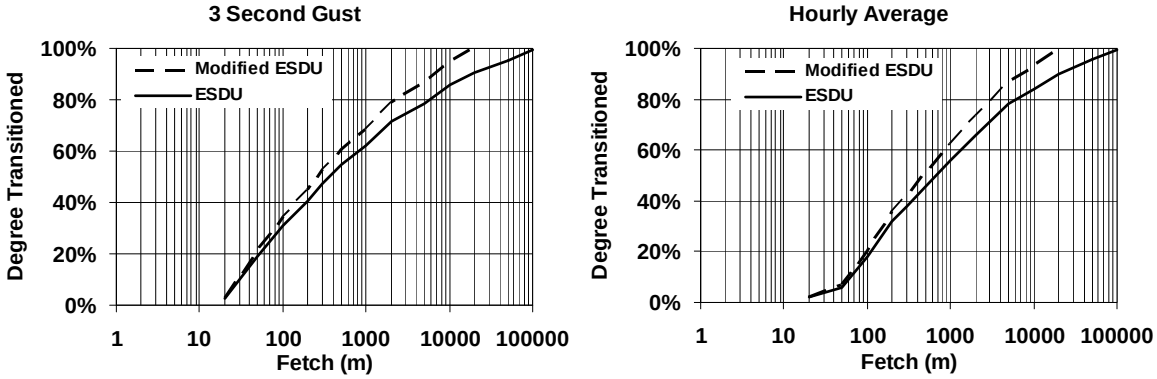

Figure 2-8. ESDU and modified ESDU wind speed transition functions at 10 m elevation.

Figure 2-9 presents a summary comparison of the maximum peak gust wind speeds computed using the wind field model described in Vickery et al. (2008b) to observations for both marine and land based anemometers. There are a total of 245 comparisons summarized in the data presented in Figure 2-9 (165 land based measurements and 80 marine based measurements). The agreement between the model and observed wind speeds is good, however there are relatively few measured gust wind speeds greater than 100 mph. The largest observed gust wind speed is only 128 mph. The differences between the modelled and observed wind speeds is caused by a combination of the inability of the wind field model to be adequately described by single values of *B* and *RMW*, errors in the modelled boundary layer, errors in height, terrain and averaging time adjustments applied to measured wind speeds (if required) as well as storm track position errors and errors in the estimated values of Δp, *RMW* and *B*. Estimates of the wind field model error obtained from the information given in Figure 2-9 are used in the estimates of wind speed as a function of return period as described in Section 3.

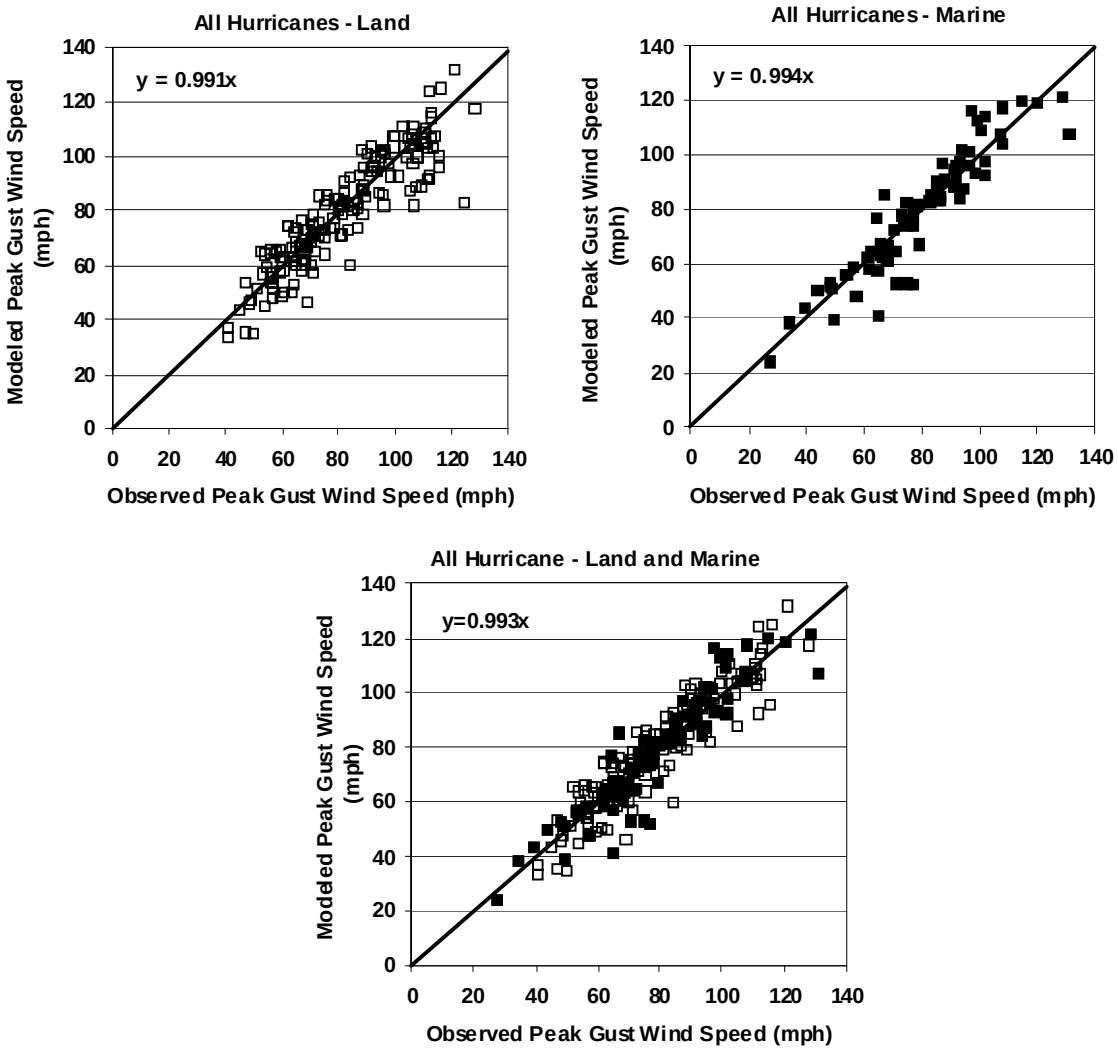

Figure 2-9. Example comparisons of modelled and observed maximum surface level peak gust wind speeds from US landfalling hurricanes. Wind speeds measured on land are given for open terrain and wind speeds measured over water are given for marine terrain.

3. DESIGN WIND SPEEDS

The hurricane simulation model described in section 2 was used to develop estimates of peak gust wind speeds as a function of return period in the Caribbean. All speeds are produced as values associated with a 3 second gust wind speed at a height of 10 m in flat open terrain. The wind speeds can be used in conjunction with the methods outlined in Chapters 2 and 6 of ASCE editions 7-98 and later for the purposes of estimating design wind pressures. As will be discussed in more detail below, the basic wind speed to be used in the design of Category II structures is the 700-year wind speed divided by $\sqrt{1.6}$. For Category III and IV structures, the wind speed to be used is the 1,700-year wind speed divided by $\sqrt{1.6}$. The use of 1,700-year wind speed divided by $\sqrt{1.6}$ replaces the need to use the 700 year values with an importance factor of 1.15 as given in ASCE 7-98 and later. For buildings located near the coast, the wind speeds presented herein should be used with the procedures given in ASCE 7 including the use of Exposure D. The use of exposure D is required because of the limit in the sea surface drag coefficient. The following sections discuss the development of the wind speed maps and the use of the resulting wind speeds in conjunction with the wind load provisions as given in ASCE 7-98 and later.

3.1 Design Wind Speed Maps

Predictions of wind speed as a function of return period at any point in the Caribbean are obtained using the hurricane simulation model described in Section 2 using a 100,000 year simulation of hurricanes. Upon completion of the 100,000-year simulation, the wind speed data are rank ordered and then used to define the wind speed probability distribution, *P(v>V)*, conditional on a storm having passed within 250 km of the site and producing a peak gust wind speed of at least 20 mph. The wind speed associated with a given exceedance probability is obtained by interpolating from the rank ordered wind speed data. The probability that the tropical cyclone wind speed (independent of direction) is exceeded during time period *t* is,

$$P_t(v > V) = 1 - \sum_{x=0}^{\infty} P(v < V \mid x)\, p_t(x) \tag{3-1}$$

where $P(v < V \mid x)$ is the probability that the velocity *v* is less than *V* given that *x* storms occur, and $p_t(x)$ is the probability of *x* storms occurring during time period *t*. From Equation 3-1, with $p_t(x)$ defined as having a Poisson distribution and defining *t* as one year, the annual probability of exceeding a given wind speed is,

$$P_a(v > V) = 1 - \exp[-\lambda P(v > V)] \tag{3-2}$$

where λ (annual occurrence rate) represents the average annual number of storms approaching within 250 km of the site and producing a minimum 20 mph peak gust wind speed, and $P(v > V)$ is the probability that the velocity *v* is greater than *V* given the occurrence of any one storm.

In order to develop wind speed contours for use in the Caribbean basin, we performed two separate simulations for:

(i) Developing a contour map of open terrain wind speeds valid for locations near the coast (i.e. small islands) generated on a 1 degree square grid encompassing the entire Caribbean basin. Each location on the 1 degree grid is treated as an "island" with a distance of 1 km to the water in all directions, thus the predicted wind speeds are representative of open terrain values for a near coast location.

(ii) Developing contour maps of wind speeds on the larger islands of the Greater Antilles (Cuba, Hispaniola, Jamaica and Puerto Rico) developed on a 10 km grid. Each grid point contains information on the distance to the coast for all (36) directions.

Wind speeds were predicted for return periods of 50, 100, 700 and 1,700 years. The 700 and 1,700 year values were computed to provide wind speeds consistent with the return periods currently implied in ASCE 7-98 and later. Appendix B provides background information as the rationale behind the selection of return periods of 700 and 1,700 years.

At each location the effect of wind field modelling uncertainty was included. The inclusion of the wind field modelling uncertainty results in an increase in the predicted wind speeds compared to the case where wind field model uncertainty is not included. The magnitude of the increased wind speeds increases with increasing return period, where the 50-, 100-, 700- and 1,700-year return period wind speeds are, on average about 1%, 2%, 4% and 5%, respectively, higher than those obtained without considering uncertainty.

The resulting hurricane hazard maps are presented in Figures 3-1 through 3-8. Figures 3-1 through 3-4 present contour maps of open terrain wind speeds for the entire Caribbean basin (except for the Greater Antilles, which are given separately in Figures 3-5 through 3-8). Apparent discontinuities between the basin contours (Figures 3-1 through 3-4) and the Greater Antilles Island contours (Figures 3-5 through 3-6) may exist because of the grid resolutions used to develop the two sets of contours (~10 km for the Greater Antilles Islands vs. ~ 100 km for the basin). An additional potential source of discontinuities is associated with the modelling of the distance to the coast, where actual distances varying with direction are used in the 10 km grid for the islands, and a simplified 1 km distance for all directions is used for the basin contours.

Wind speeds at representative locations on the populated islands are summarized in Table 3-1. Each of these island locations are treated as point locations with a distance of 1 km to the water in all directions, thus the predicted wind speeds are representative of open terrain values for a near coast location, and are consistent with the wind speeds used to develop the contours given in Figures 3-1 through 3-4.

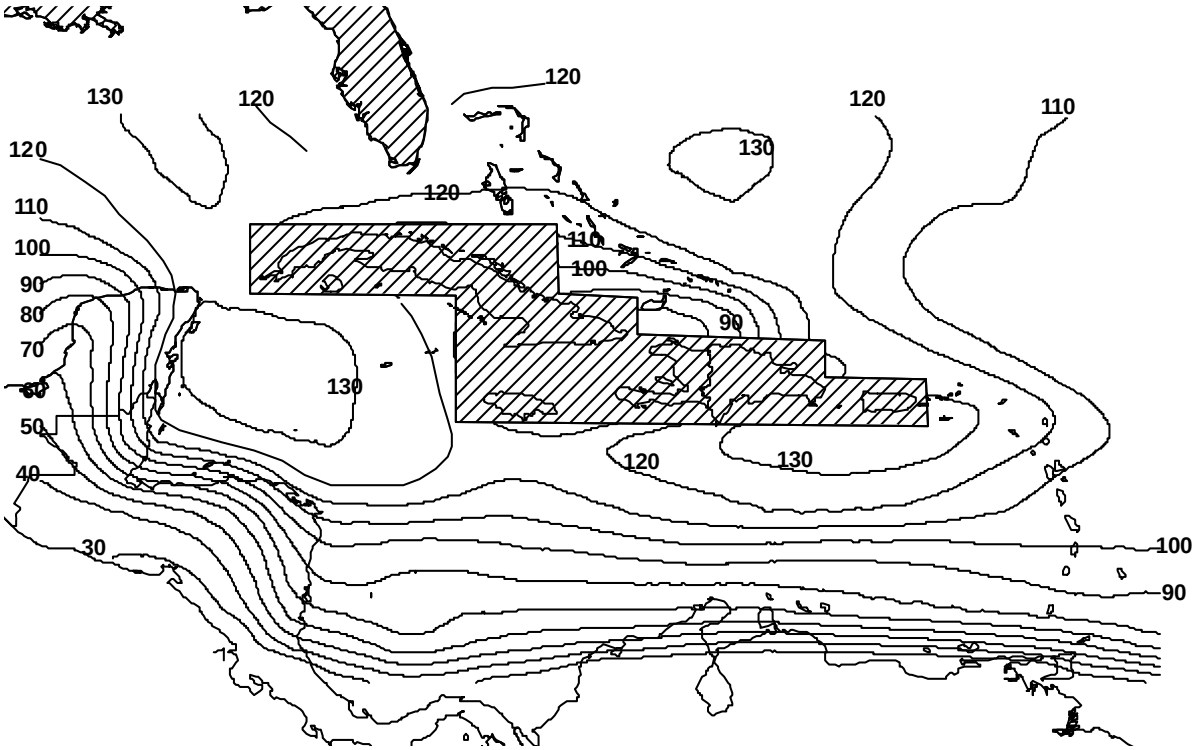

Figure 3-1. Contours or predicted 50 year return period peak gust wind speeds (mph) at a height of 10m in flat open terrain (ASCE 7 Exposure C).

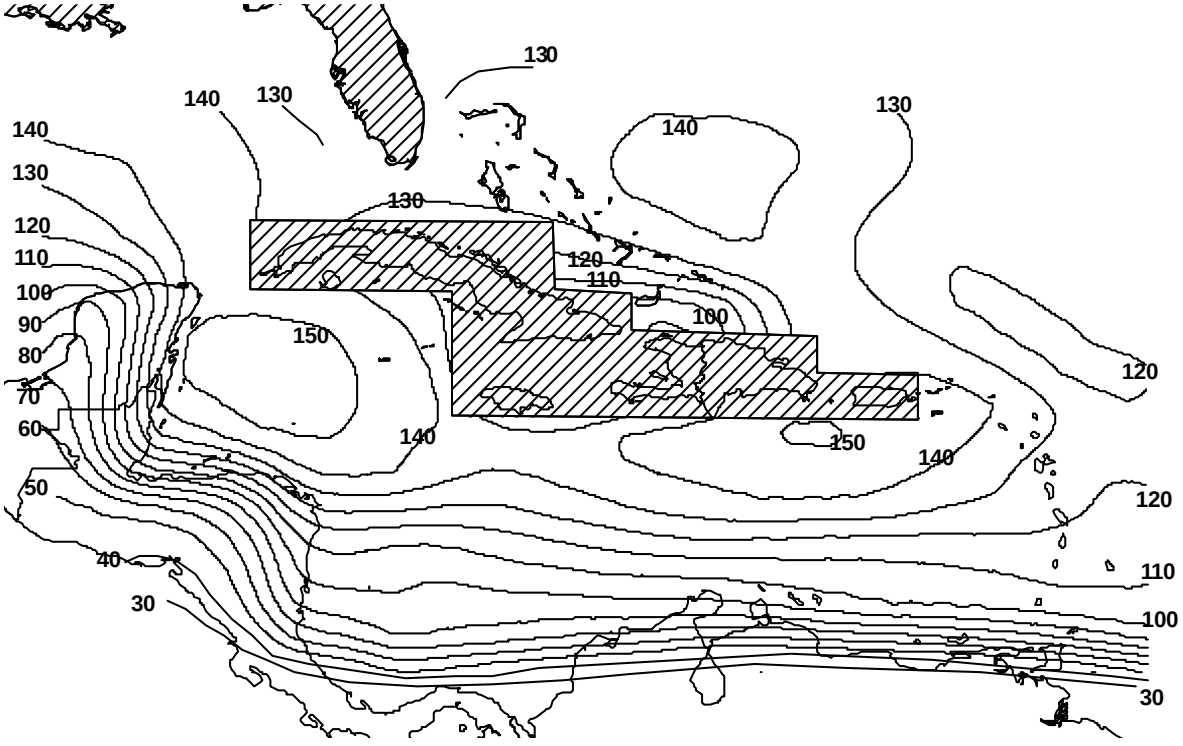

Figure 3-2. Contours or predicted 100 year return period peak gust wind speeds (mph) at a height of 10m in flat open terrain (ASCE 7 Exposure C).

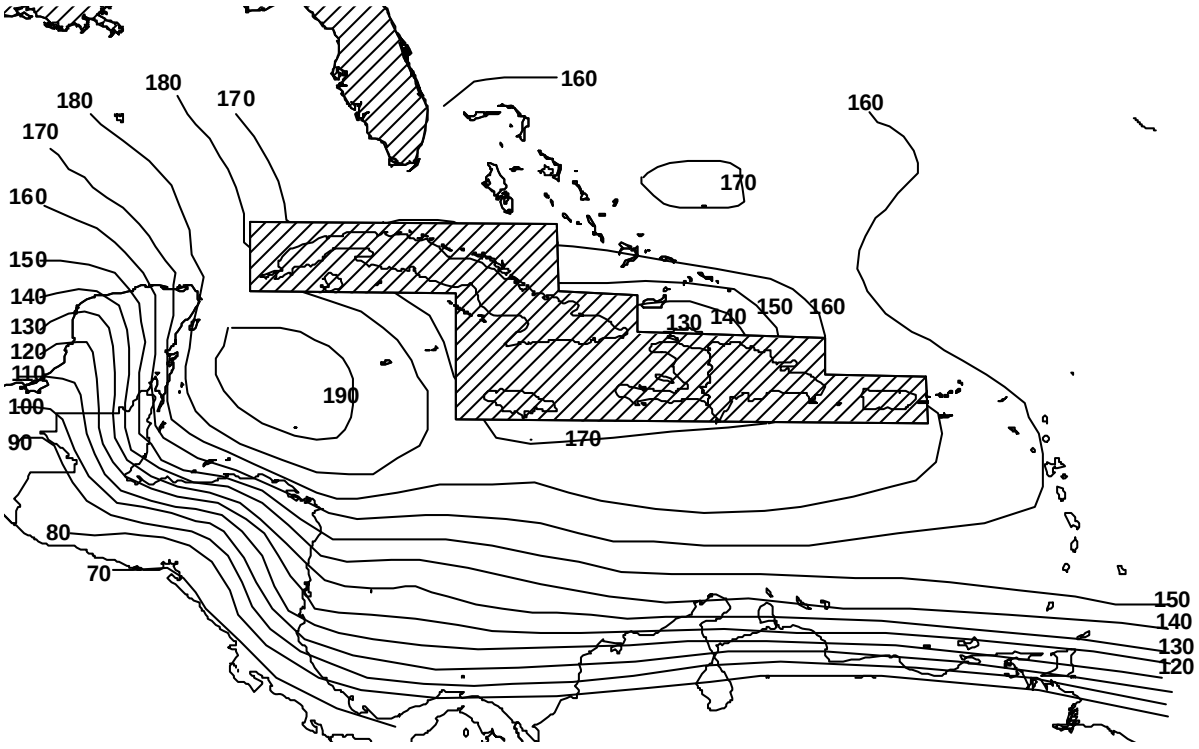

Figure 3-3. Contours or predicted 700 year return period peak gust wind speeds (mph) at a height of 10m in flat open terrain (ASCE 7 Exposure C).

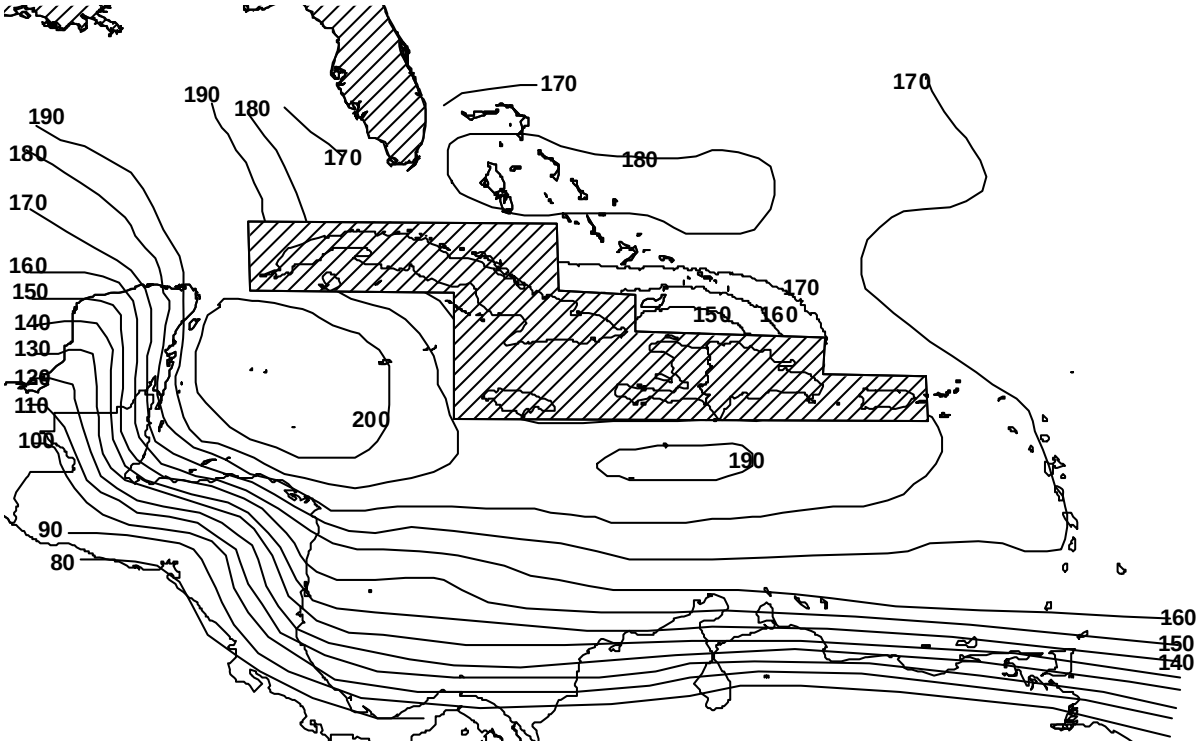

Figure 3-4. Contours or predicted 1,700 year return period peak gust wind speeds (mph) at a height of 10m in flat open terrain (ASCE 7 Exposure C).

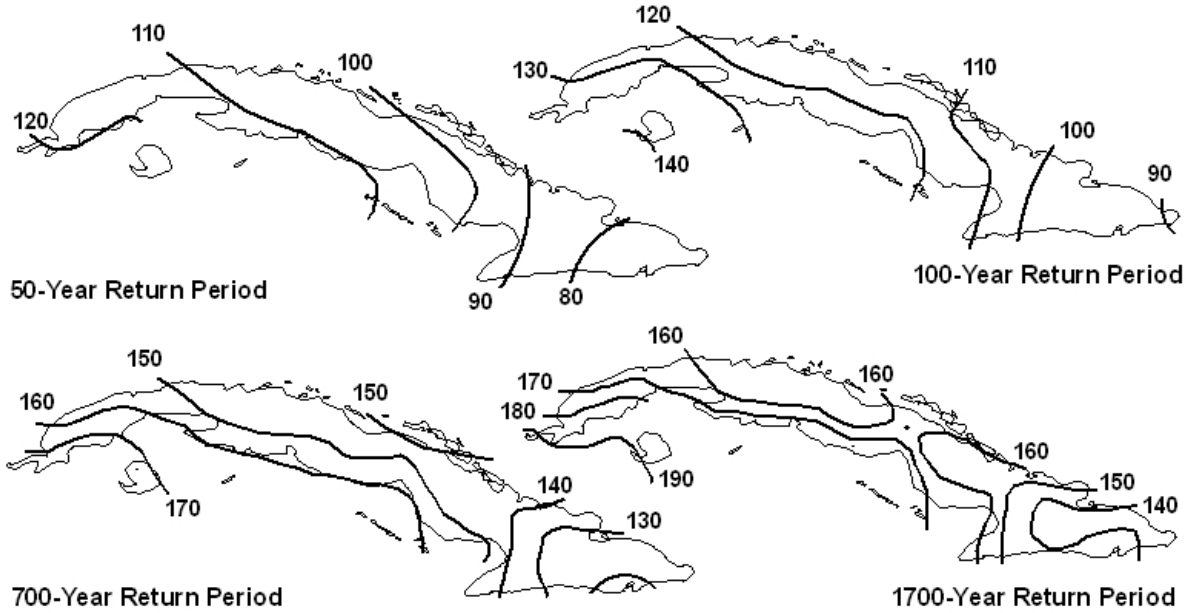

Figure 3-5. Contours of period peak gust wind speeds (mph) at a height of 10m in flat open terrain for various return periods for Cuba (ASCE 7 Exposure C).

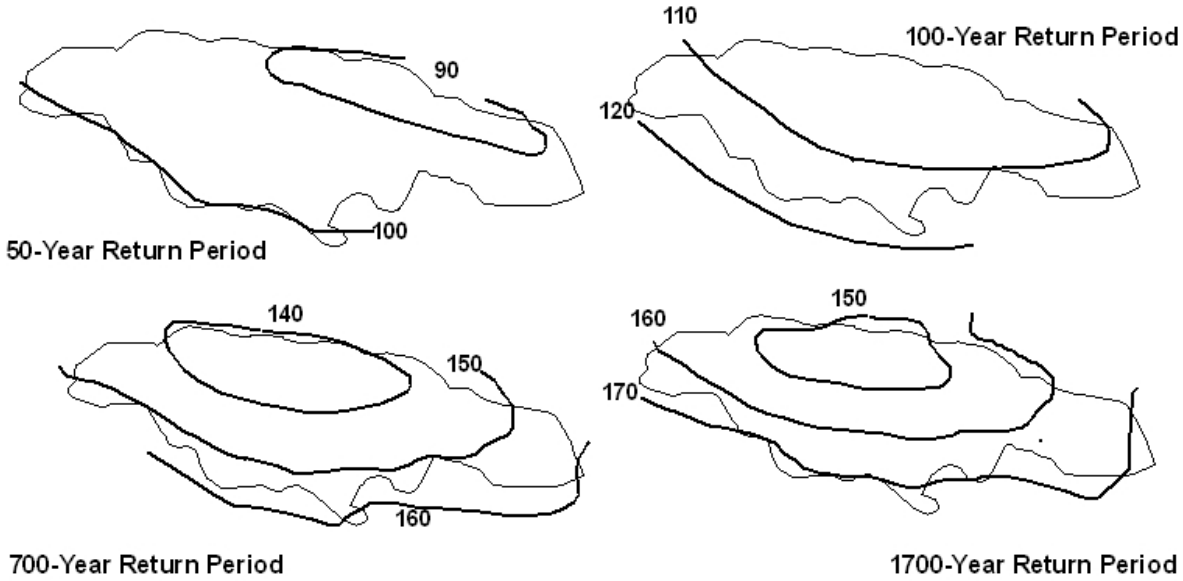

Figure 3-6. Contours of period peak gust wind speeds (mph) at a height of 10m in flat open terrain for various return periods for Jamaica (ASCE 7 Exposure C).

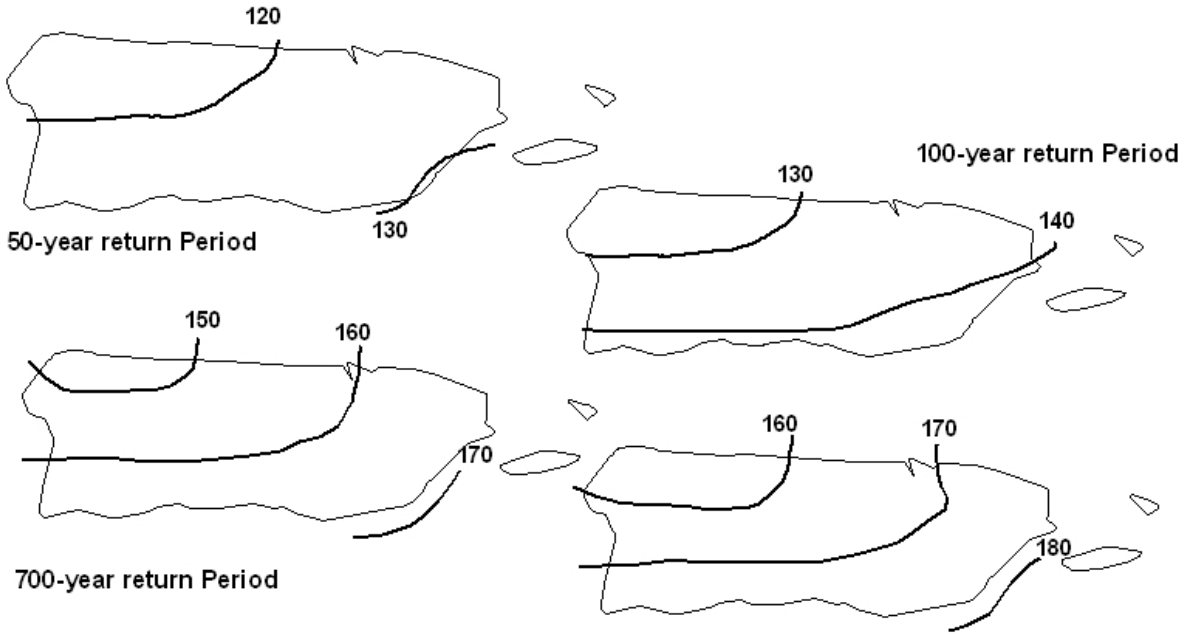

Figure 3-7. Contours of period peak gust wind speeds (mph) at a height of 10m in flat open terrain for various return periods for Puerto Rico (ASCE 7 Exposure C).

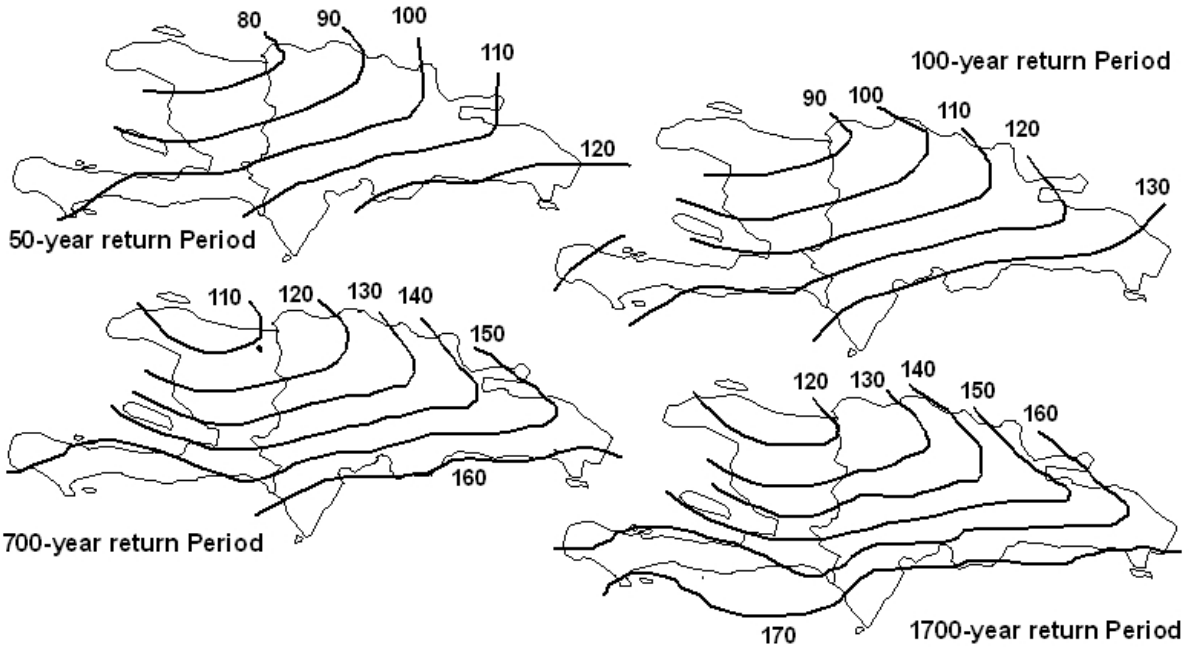

Figure 3-8. Contours of period peak gust wind speeds (mph) at a height of 10m in flat open terrain for various return periods for the island of Hispaniola(ASCE 7 Exposure C).

Table 3-1 Peak gust wind speeds (mph) in flat open terrain (ASCE 7 Exposure C) as a function of return period for selected locations in the Caribbean

Location	Lat	Long	Return Period (years)			
			50	100	700	1700
Trinidad (S)	10.03	61.33	19	32	82	102
Trinidad (N)	11.20	61.33	61	85	136	156
Isla Margarita	10.50	64.17	24	42	100	128
Grenada	12.12	61.67	85	107	154	168
Bonaire	12.25	68.28	77	101	149	156
Curacao	12.17	69.55	73	96	147	168
Aruba	12.53	70.03	77	100	146	162
Barbados	13.08	59.50	92	112	152	169
Saint Vincent	13.17	61.17	93	111	155	171
Saint Lucia	14.03	60.97	101	119	155	172
Martinique	14.60	61.03	104	121	159	171
Dominica	15.42	61.33	106	124	159	172
Guadeloupe	16.00	61.73	110	126	157	168
Montserrat	16.75	62.70	120	135	164	172
St. Kitts and Nevis	17.33	62.75	125	138	163	170
Antigua and Barbuda	17.33	61.80	121	134	160	168
Saint Martin/Sint Maarten	17.98	63.17	129	141	168	178
Anguilla	18.25	63.17	127	140	166	176
US Virgin Islands	18.35	64.93	130	143	167	176
British Virgin Islands	18.45	64.62	128	141	169	180
Grand Cayman	19.33	81.40	128	147	187	200
Little Cayman/Cayman Brac	19.72	79.82	118	136	178	197
Turks & Caicos (Grand Turk)	21.47	71.13	105	120	150	162
Turks & Caicos (Providenciales)	21.77	72.27	110	124	155	170
Eleuthera	24.96	76.45	122	135	165	180
Andros	24.29	77.68	120	132	162	180
New Providence (Nassau)	25.04	77.46	121	132	163	180
Great Abaco	26.45	77.30	121	133	162	178
Grand Bahama (Freeport)	26.55	78.70	120	132	161	175
Belmopan, Belize	17.15	88.45	106	128	165	177

3.2 Use of Wind Speeds with ASCE 7 Wind Loading Criteria

The wind speeds presented herein can be used with the wind loading requirements given in ASCE 7 (ASCE 7-98 and later) to compute wind loads for the design of buildings and structures as described in the following section. The velocity pressure, q_z (psf), given in ASCE 7 is defined as:

$$q_z = 0.00256 K_z K_{zt} K_d V^2 I \qquad (3\text{-}3)$$

where K_d is a wind directionality factor, K_{zt} is a height dependent topographic factor, K_z is a velocity pressure exposure coefficient, V is the basic design wind speed (*not the 50 year return period wind speed*) and has the units of mph, and I is an importance factor. Again, the units of q_z are pounds per square foot and the units of the wind speed are miles per hour. The wind speed information presented herein can be used to define the basic wind speed, V and the importance factor, I. The importance factor, I is approximately equal to the square of the ratio of the 100 year return period wind speed in a non-hurricane prone region divided by the 50 year return period wind speed in the non-hurricane prone regions of the United States.

As discussed in the commentaries of ASCE 7-98, ASCE 7-02 and ASCE 7-05, and Appendix B of this report, the basic wind speed used in ASCE 7 is the 500-year return period wind speed divided by $\sqrt{1.5}$. In the non-hurricane prone region of the US, the resulting basic wind speed is a 50-year return period value. In the hurricane prone regions of the continental United States the return period associated with the basic wind speed varies with location, but is typically in the range of 70 to 100 years.

Here, the basic wind speed is the 700-year return period wind speed divided by $\sqrt{1.6}$, which yields a design wind speed that is consistent with the intent of the developers of the ASCE 7 wind speed map. Thus the wind speed to be used in Equation 3-3 and subsequently the wind load calculations given in ASCE 7 is

$$V = V_{700} / \sqrt{1.6}$$

Appendix B provides information as to the reason for using a 700-year return period wind speed divided by $\sqrt{1.6}$, as compared to the 500 year return period wind speed divided by $\sqrt{1.5}$ as presented in ASCE 7-98 through ASCE 7-05. Appendix B also provides the rationale for replacing the $V^2 I$ term (where I =1.15) in Equation 3-3 with $(V_{1700} / \sqrt{1.6})^2$ for the design of Category III and IV structures.

4. SUMMARY

Estimates of wind speeds as a function of return period for locations in the Caribbean basin were developed using a peer reviewed hurricane simulation model as described in Vickery et al. (2000a, 2000b, 2008a, 2008b), Vickery and Wadhera, (2008).

Maps of hurricane induced wind speeds were generated. The hurricane simulation model used here is an updated version of that described in Vickery et al. (2000a, 2000b) which was used to produce the design wind speeds used in the ASCE 7-98 through to the ASCE 7-05, the most current version.

All wind speeds produced are 3 second gust wind speeds at a height of 10 m in flat open terrain. The wind speeds can be used in conjunction with the methods outlined in Chapters 2 and 6 of ASCE Editions 7-98 and later for the purposes of estimating design wind pressures. The basic wind speed to be used in the design of Category II structures is the 700 year wind speed divided by $\sqrt{1.6}$. For Category III and IV structures, the wind speed to be used should be the 1700 year wind speed divided by $\sqrt{1.6}$. The use of 1700 year wind speed divided by $\sqrt{1.6}$ replaces the need to use the 700 year values with an importance factor of 1.15 as given in ASCE-7.

For buildings located near the coast, the wind speeds presented herein should be used with the procedures given in ASCE 7 including the use of exposure D. The use of exposure D is required because of the limit in the sea surface drag coefficient.

5. REFERENCES

Donelan, M.A., B.K. Haus, N. Reul, W.J. Plant, M. Stiassnie, H.C. Graber, O.B. Brown, and E.S. Saltzman, (2004). "On the limiting aerodynamic roughness in the ocean in very strong winds" *Geophys. Res. Lett.*, **31,** L18306

Emanuel, K.A, S. Ravela, E. Vivant and C. Risi, (2006), "A statistical–deterministic approach to hurricane risk assessment", *Bull. Amer. Meteor. Soc*., **19**, 299-314.

ESDU, (1982), "Strong Winds in the Atmospheric Boundary Layer, Part 1: Mean Hourly Wind Speed", Engineering Sciences Data Unit Item No. 82026, London, England, 1982.

Georgiou, P.N., (1985), "Design Windspeeds in Tropical Cyclone-Prone Regions", Ph.D. Thesis, Faculty of Engineering Science, University of Western Ontario, London, Ontario, Canada, 1985.

Georgiou, P.N., A.G. Davenport and B.J. Vickery, (1983) "Design wind speeds in regions dominated by tropical cyclones", 6th International Conference on Wind Engineering, Gold Coast, Australia, 21-25 March and Auckland, New Zealand, 6-7 April.

Holland, G.J., (1980), "An analytic model of the wind and pressure profiles in hurricanes, *Mon. Wea. Rev*., **108** (1980) 1212-1218.

James, M. K. and L.B. Mason, (2005), "Synthetic tropical cyclone database", *J. Wtrwy, Port, Coast and Oc. Engrg.*, **131,** 181-192

Jarvinen, B.R., C.J. Neumann, and M.A.S. Davis, (1984), "A Tropical Cyclone Data Tape for the North Atlantic Basin 1886-1983: Contents, Limitations and Uses", NOAA Technical Memorandum NWS NHC 22, U.S. Department of Commerce, March, 1984.

DeMaria, M., and J. Kaplan (1999), "An updated Statistical Hurricane Intensity Prediction Scheme (SHIPS) for the Atlantic and Eastern North Pacific Basins", *Weather and Forecasting*, **14**, 326–337.

Powell, M.D., P.J. Vickery, and T.A. Reinhold, (2003), "Reduced drag coefficient for high wind speeds in tropical cyclones", *Nature*, **422,** 279-283.

Simiu, E., P. J. Vickery, and A Kareem, (2007), "Relations between Saffir-Simpson hurricane scale wind speeds and peak 3-s gust speeds over open terrain", *J. Struct. Eng*, **133**, 1043-1045

Vickery, P.J. and D. Wadhera, (2008), "Statistical Models of Holland Pressure Profile Parameter and Radius to Maximum Winds of Hurricanes from Flight Level Pressure and H*Wind Data", submitted to *J. Appl. Meteor.*

Vickery, P.J.; D. Wadhera, L.A. Twisdale Jr., and F.M. Lavelle, (2008a), "United States hurricane wind speed risk and uncertainty", submitted to *J. Struct. Eng.*.

Vickery, P.J., D. Wadhera, M.D. Powell and Y. Chen, (2008b) "A Hurricane Boundary Layer and Wind Field Model for Use in Engineering Applications", accepted for publication in *J. Appl. Meteor.*

Vickery, P.J., J. X. Lin, P. F. Skerlj, and L. A. Twisdale Jr., (2006), "The HAZUS-MH hurricane model methodology part I: Hurricane hazard, terrain and wind load modelling", *Nat. Hazards Rev.*, **7**, 82-93

Vickery, P.J., (2005), "Simple empirical models for estimating the increase in the central pressure of tropical cyclones after landfall along the coastline of the United States", *J. Appl. Meteor*., **44,** 1807-1826.

Vickery, P.J., P.F. Skerlj and L.A. Twisdale Jr., (2000a) "Simulation of hurricane risk in the U.S. using an empirical track model," *J. Struct. Eng.*, **126**, 1222-1237

Vickery, P.J., P.F. Skerlj, A.C. Steckley and L.A. Twisdale Jr., (2000b) Hurricane wind field model for use in hurricane simulations, *J. Struct. Eng.*, **126**. 1203-1221

Vickery, P.J. and P.F. Skerlj, (2000), "Elimination of exposure D along hurricane coastline in ASCE 7", *J. Struct. Eng.*. **126**, 545-549

Vickery, P.J., and L.A. Twisdale, (1995), "Prediction of hurricane wind speeds in the U.S.," *J. Struct. Eng.*, **121**, 1691-1699

Appendix A

Comparisons of modelled and observed cumulative frequency distributions of central pressure, heading, and translational speed

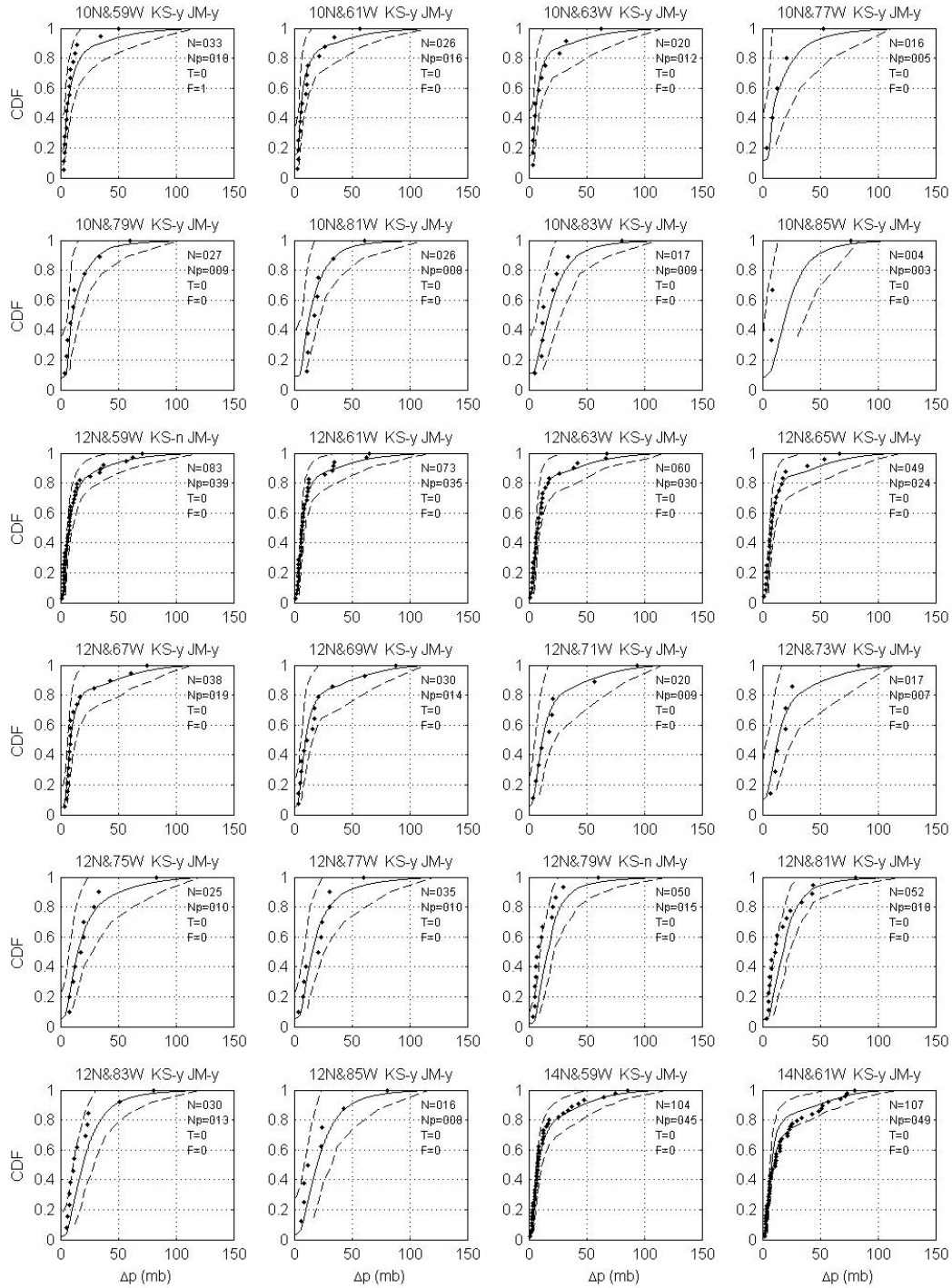

Figure A1. Comparison of modelled and observed (1900-2006) central pressure difference, minimum in a 250 km radius circle, at specific locations. Dotted lines show 90% confidence range derived from the modelled empirical distribution. N equals the total number of data points, N_p equals number of points with known central pressure, F=1 indicates failure of *F*-test, T=1 indicates failure of *T*-test, *KS*=n indicates failure of the *KS*-test, and JM=n indicates failure of the James & Mason (2005) test.

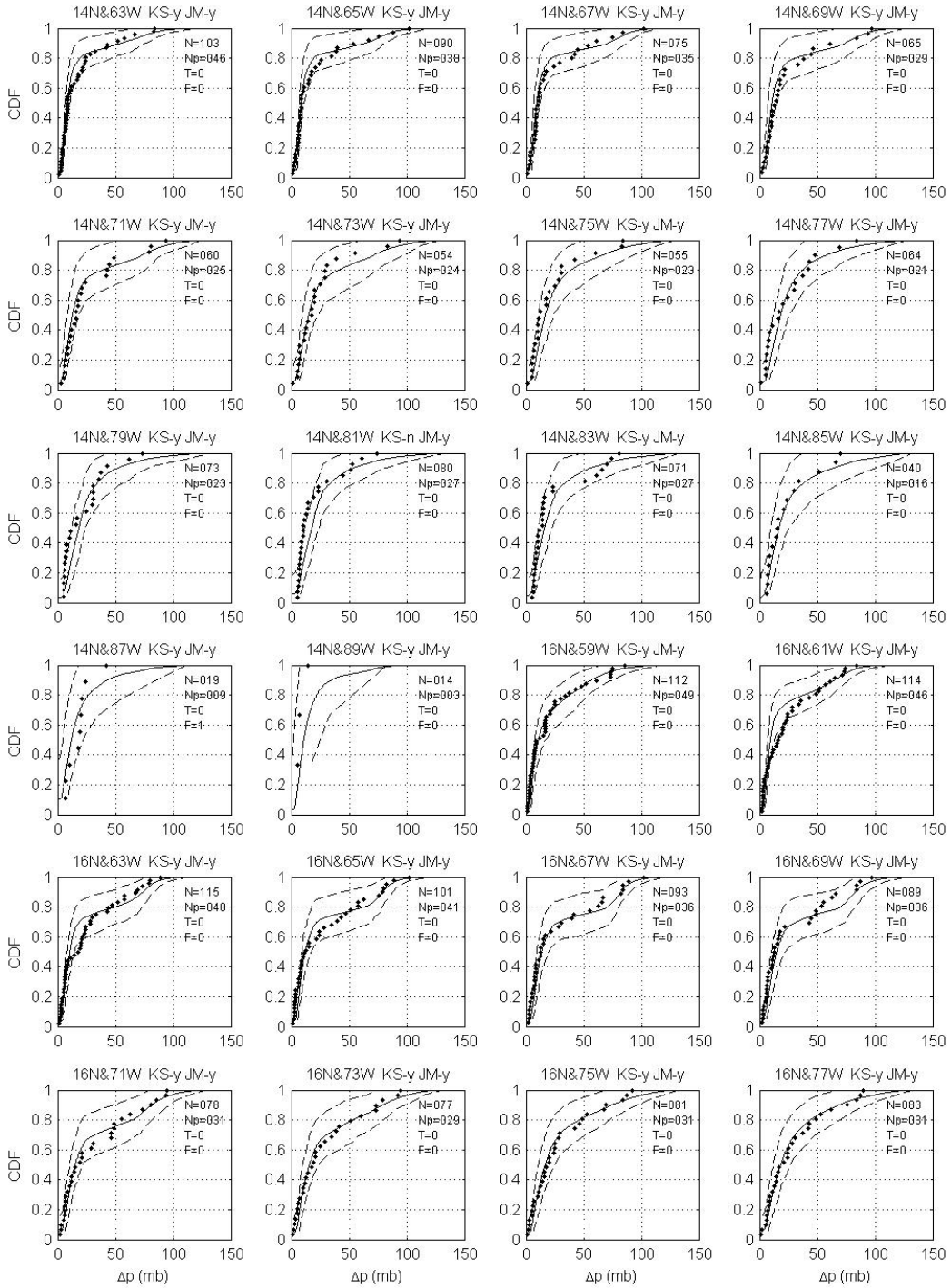

Figure A1. (Continued) Comparison of modelled and observed (1900-2006) central pressure difference, minimum in a 250 km radius circle, at specific locations. Dotted lines show 90% confidence range derived from the modelled empirical distribution. N equals the total number of data points, N_p equals number of points with known central pressure, F=1 indicates failure of *F*-test, T=1 indicates failure of *T*-test, *KS*=n indicates failure of the *KS*-test, and JM=n indicates failure of the James & Mason (2005) test.

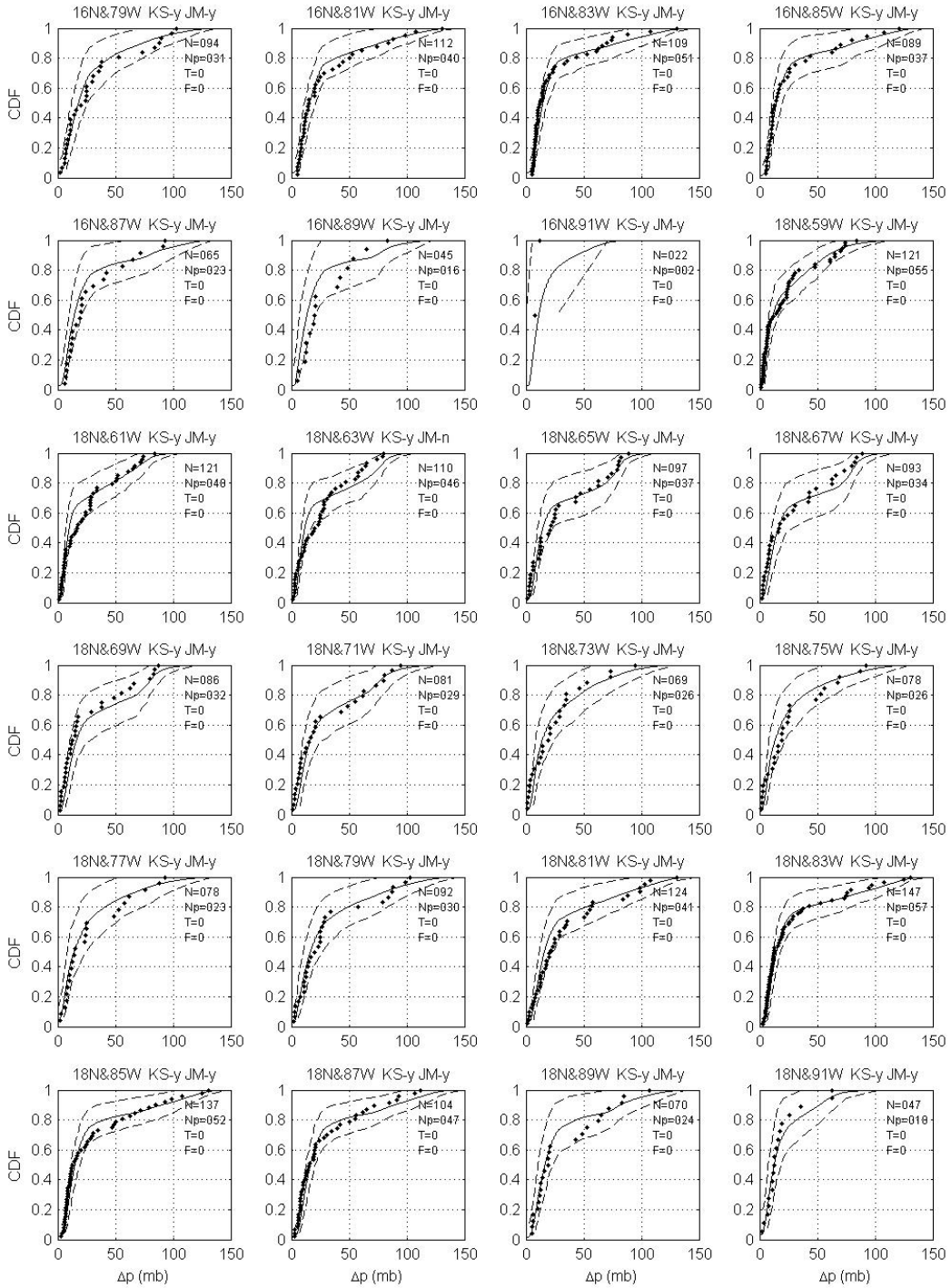

Figure A1. (Continued) Comparison of modelled and observed (1900-2006) central pressure difference, minimum in a 250 km radius circle, at specific locations. Dotted lines show 90% confidence range derived from the modelled empirical distribution. N equals the total number of data points, N_p equals number of points with known central pressure, F=1 indicates failure of *F*-test, T=1 indicates failure of *T*-test, *KS*=n indicates failure of the *KS*-test, and JM=n indicates failure of the James & Mason (2005) test.

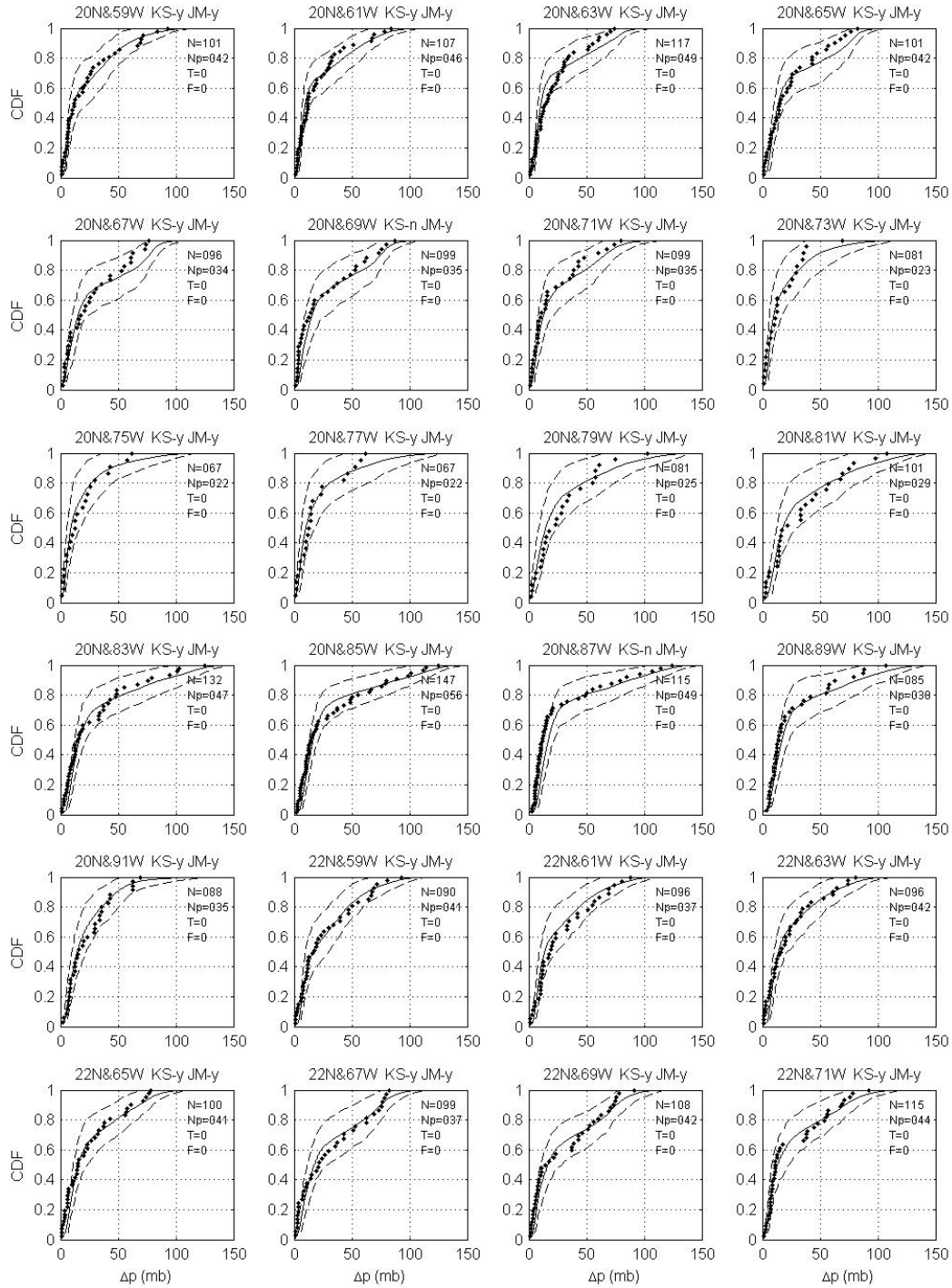

Figure A1. (Continued) Comparison of modelled and observed (1900-2006) central pressure difference, minimum in a 250 km radius circle, at specific locations. Dotted lines show 90% confidence range derived from the modelled empirical distribution. N equals the total number of data points, N_p equals number of points with known central pressure, F=1 indicates failure of *F*-test, T=1 indicates failure of *T*-test, *KS*=n indicates failure of the *KS*-test, and JM=n indicates failure of the James & Mason (2005) test.

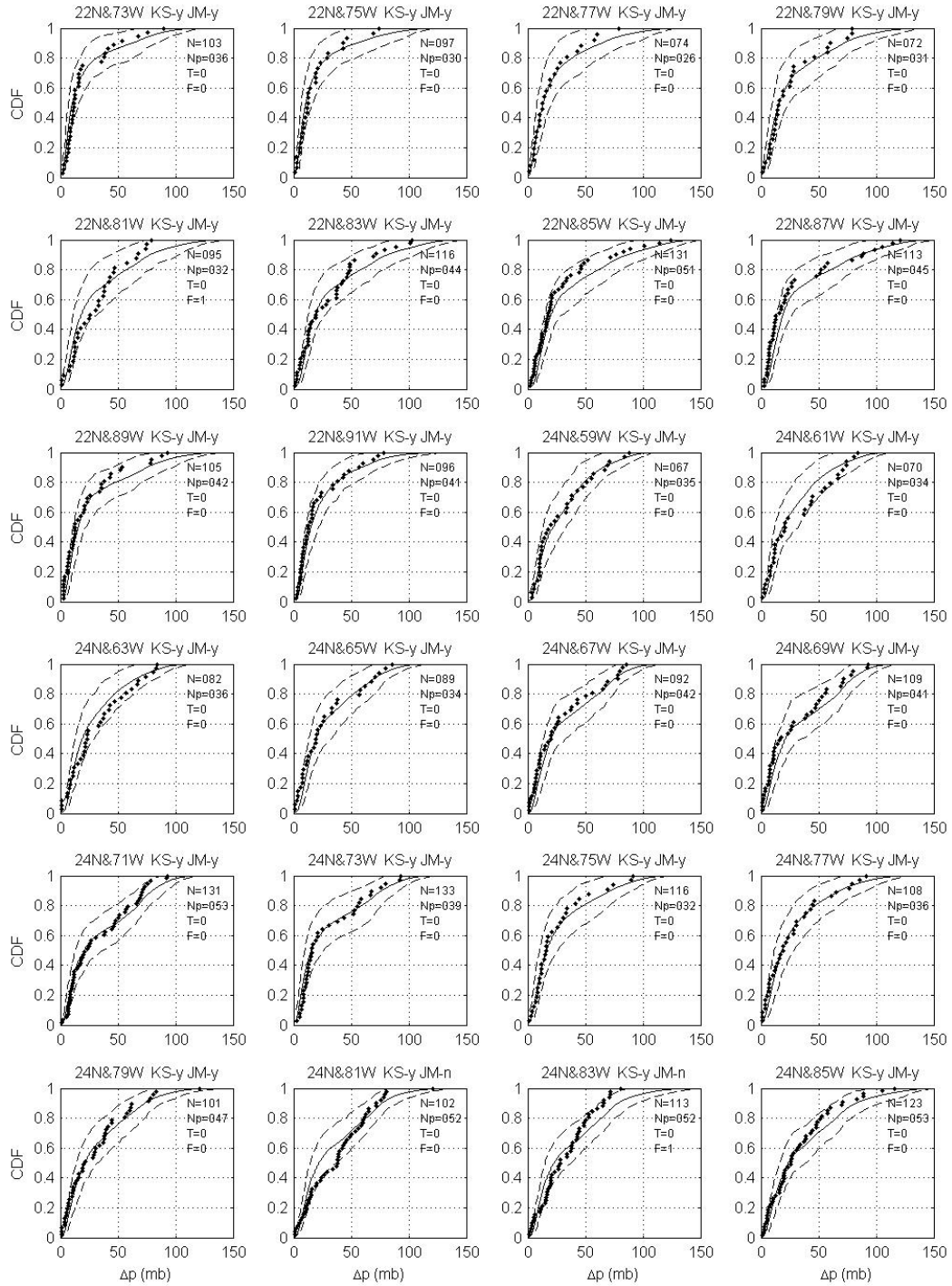

Figure A1. (Continued) Comparison of modelled and observed (1900-2006) central pressure difference, minimum in a 250 km radius circle, at specific locations. Dotted lines show 90% confidence range derived from the modelled empirical distribution. N equals the total number of data points, N_p equals number of points with known central pressure, F=1 indicates failure of *F*-test, T=1 indicates failure of *T*-test, *KS*=n indicates failure of the *KS*-test, and JM=n indicates failure of the James & Mason (2005) test.

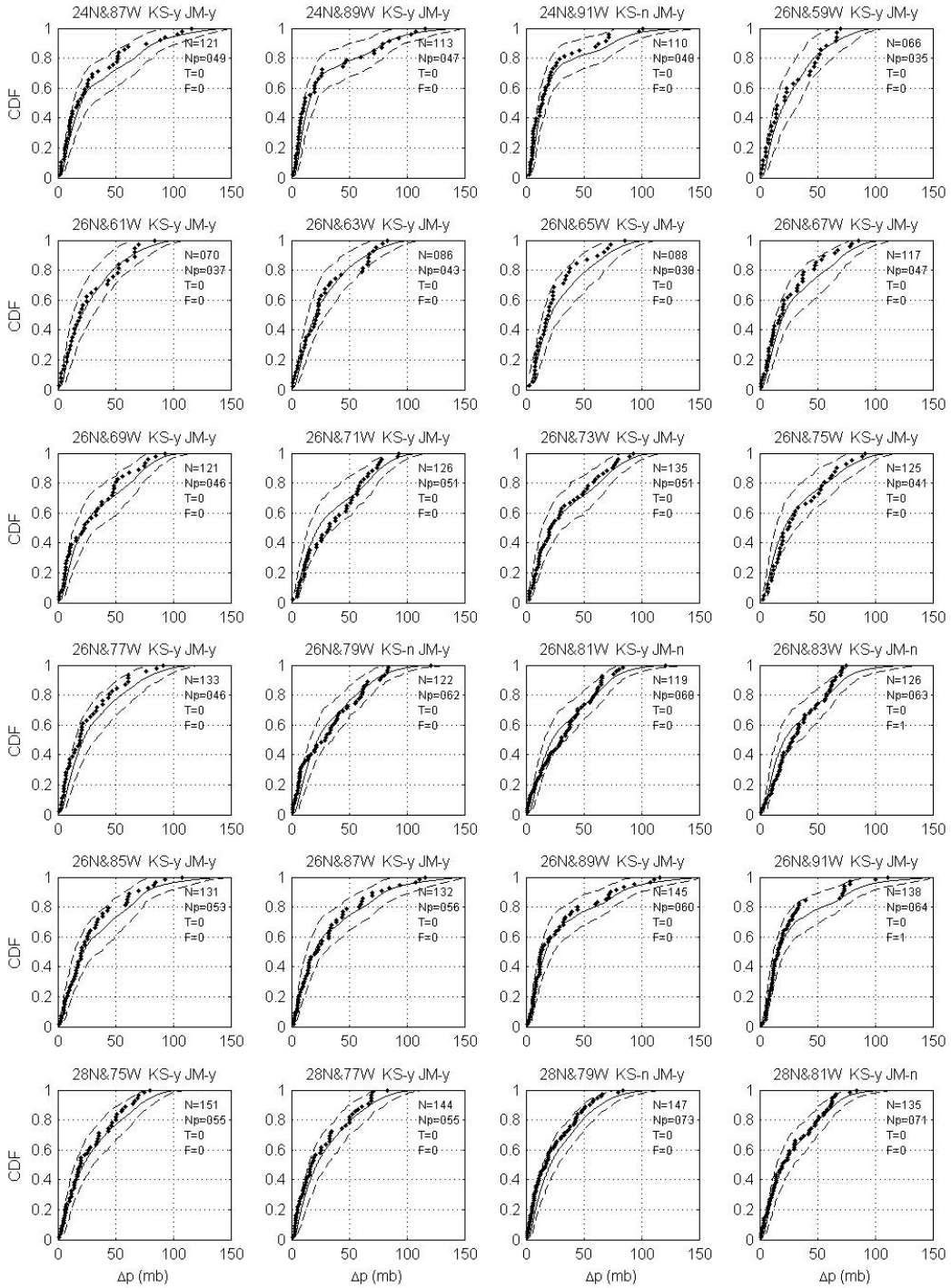

Figure A1. (Continued) Comparison of modelled and observed (1900-2006) central pressure difference, minimum in a 250 km radius circle, at specific locations. Dotted lines show 90% confidence range derived from the modelled empirical distribution. N equals the total number of data points, N_p equals number of points with known central pressure, F=1 indicates failure of *F*-test, T=1 indicates failure of *T*-test, *KS*=n indicates failure of the *KS*-test, and JM=n indicates failure of the James & Mason (2005) test.

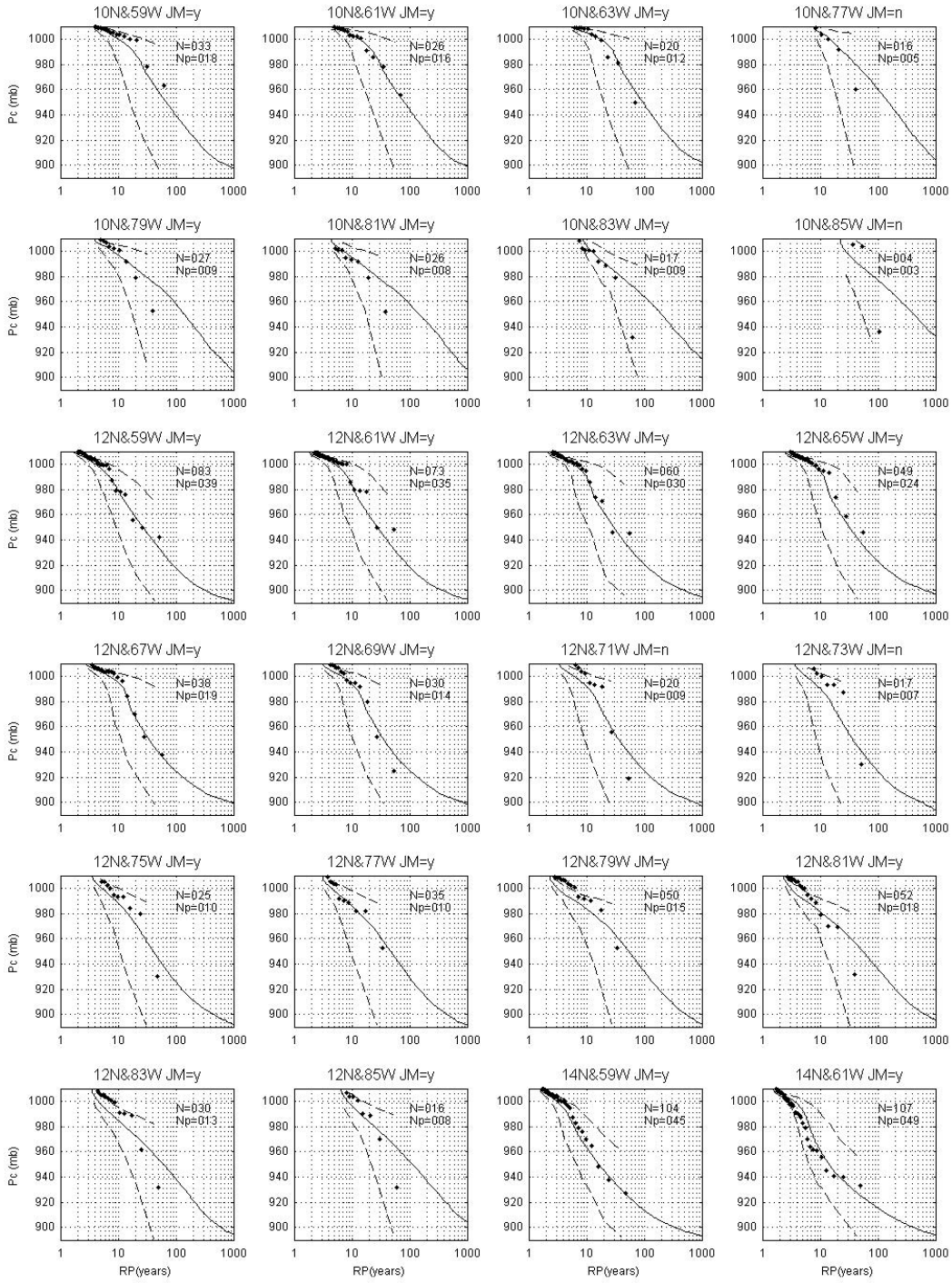

Figure A2. Comparison of modelled and observed (1900-2006) central pressures, minimum noted in a 250 km circle around a location, versus return period. Dotted lines show 90% confidence range derived from the modelled empirical distribution. N equals the total number of data points, N_p equals number of points with known central pressure, and JM=n indicates failure of the James & Mason (2005) test.

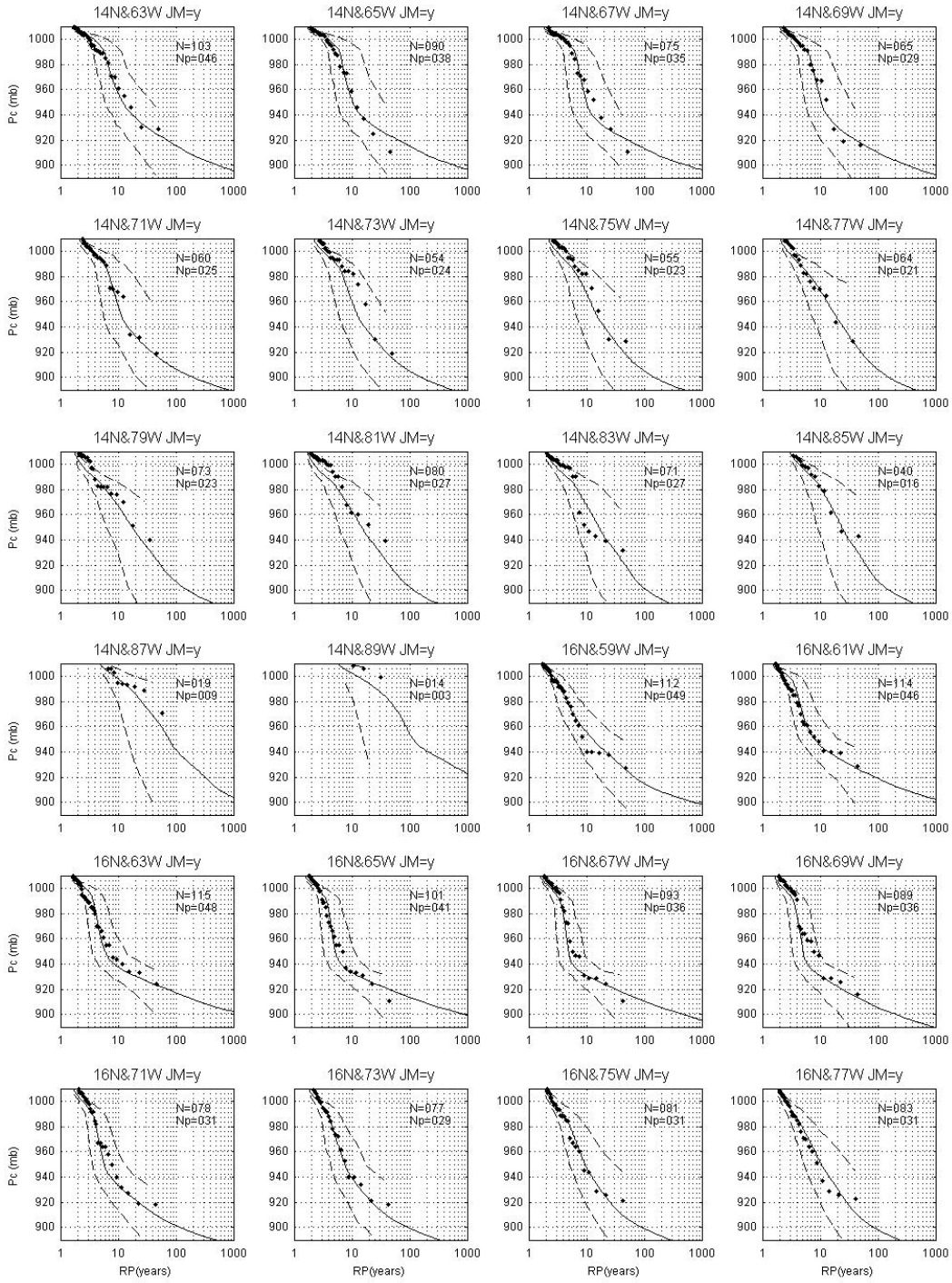

Figure A2. (Continued) Comparison of modelled and observed (1900-2006) central pressures, minimum noted in a 250 km circle around a location, versus return period. Dotted lines show 90% confidence range derived from the modelled empirical distribution. N equals the total number of data points, N_p equals number of points with known central pressure, and JM=n indicates failure of the James & Mason (2005) test.

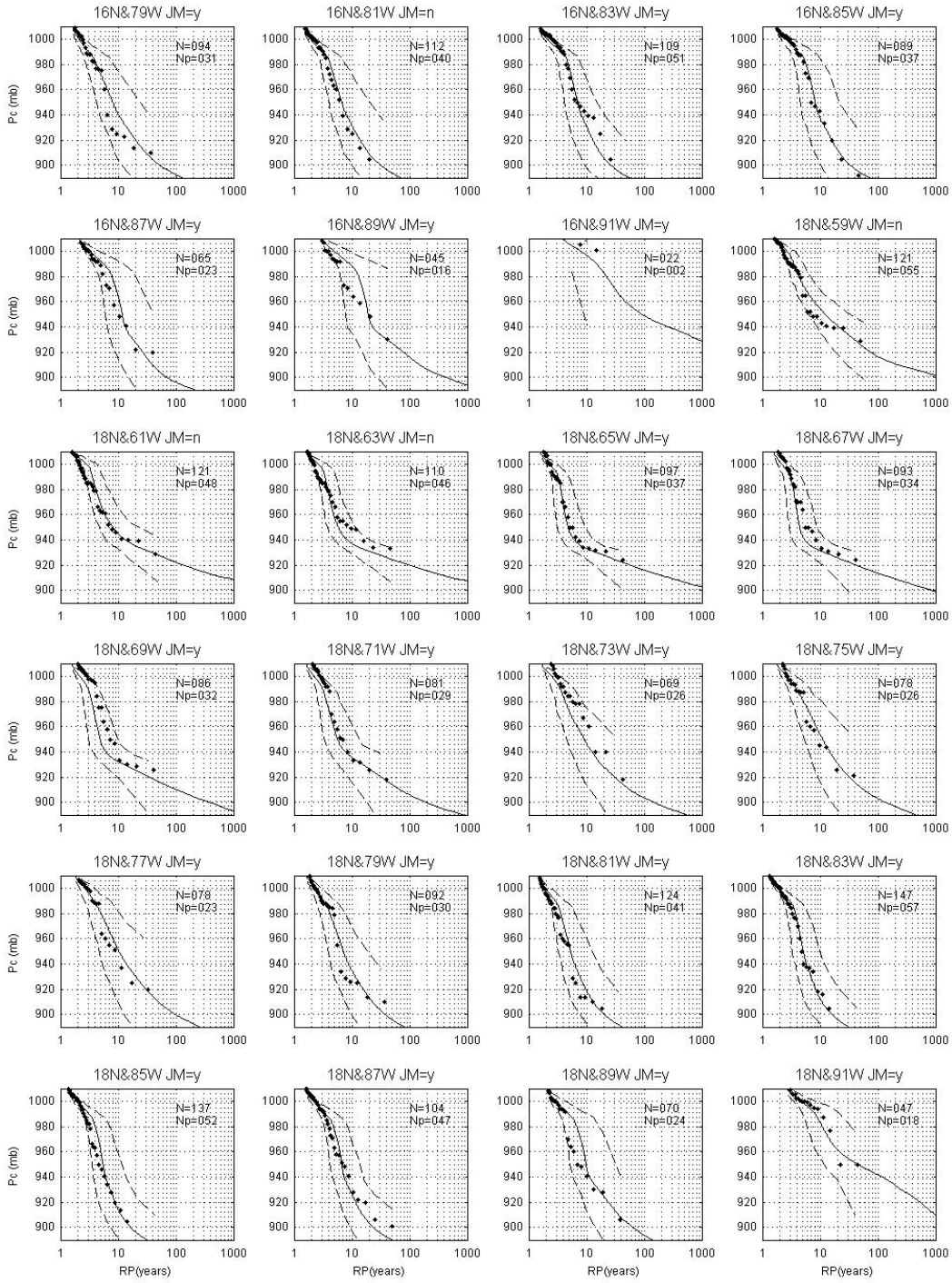

Figure A2. (Continued) Comparison of modelled and observed (1900-2006) central pressures, minimum noted in a 250 km circle around a location, versus return period. Dotted lines show 90% confidence range derived from the modelled empirical distribution. N equals the total number of data points, N_p equals number of points with known central pressure, and JM=n indicates failure of the James & Mason (2005) test.

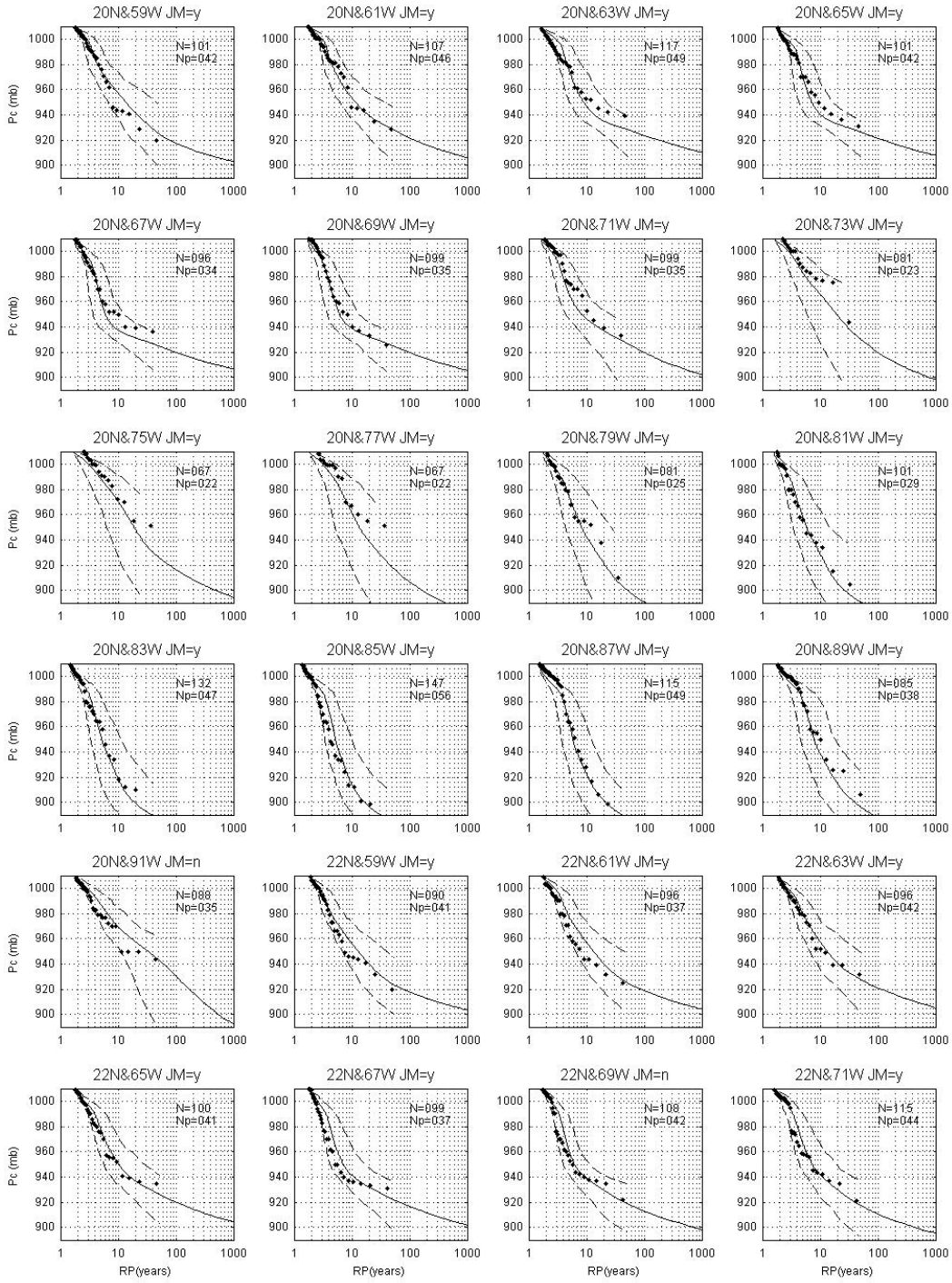

Figure A2. (Continued) Comparison of modelled and observed (1900-2006) central pressures, minimum noted in a 250 km circle around a location, versus return period. Dotted lines show 90% confidence range derived from the modelled empirical distribution. N equals the total number of data points, N_p equals number of points with known central pressure, and JM=n indicates failure of the James & Mason (2005) test.

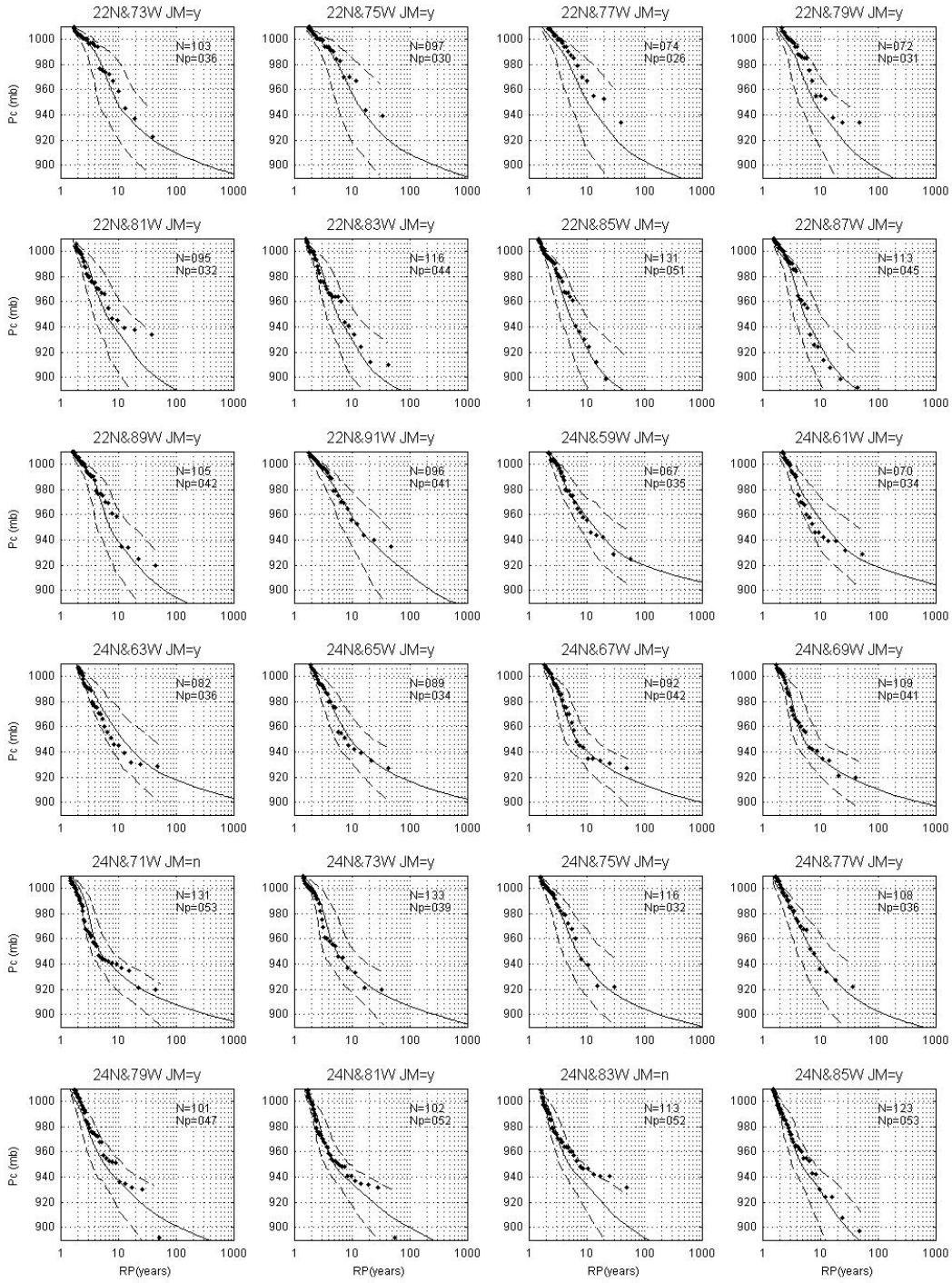

Figure A2. (Continued) Comparison of modelled and observed (1900-2006) central pressures, minimum noted in a 250 km circle around a location, versus return period. Dotted lines show 90% confidence range derived from the modelled empirical distribution. N equals the total number of data points, N_p equals number of points with known central pressure, and JM=n indicates failure of the James & Mason (2005) test.

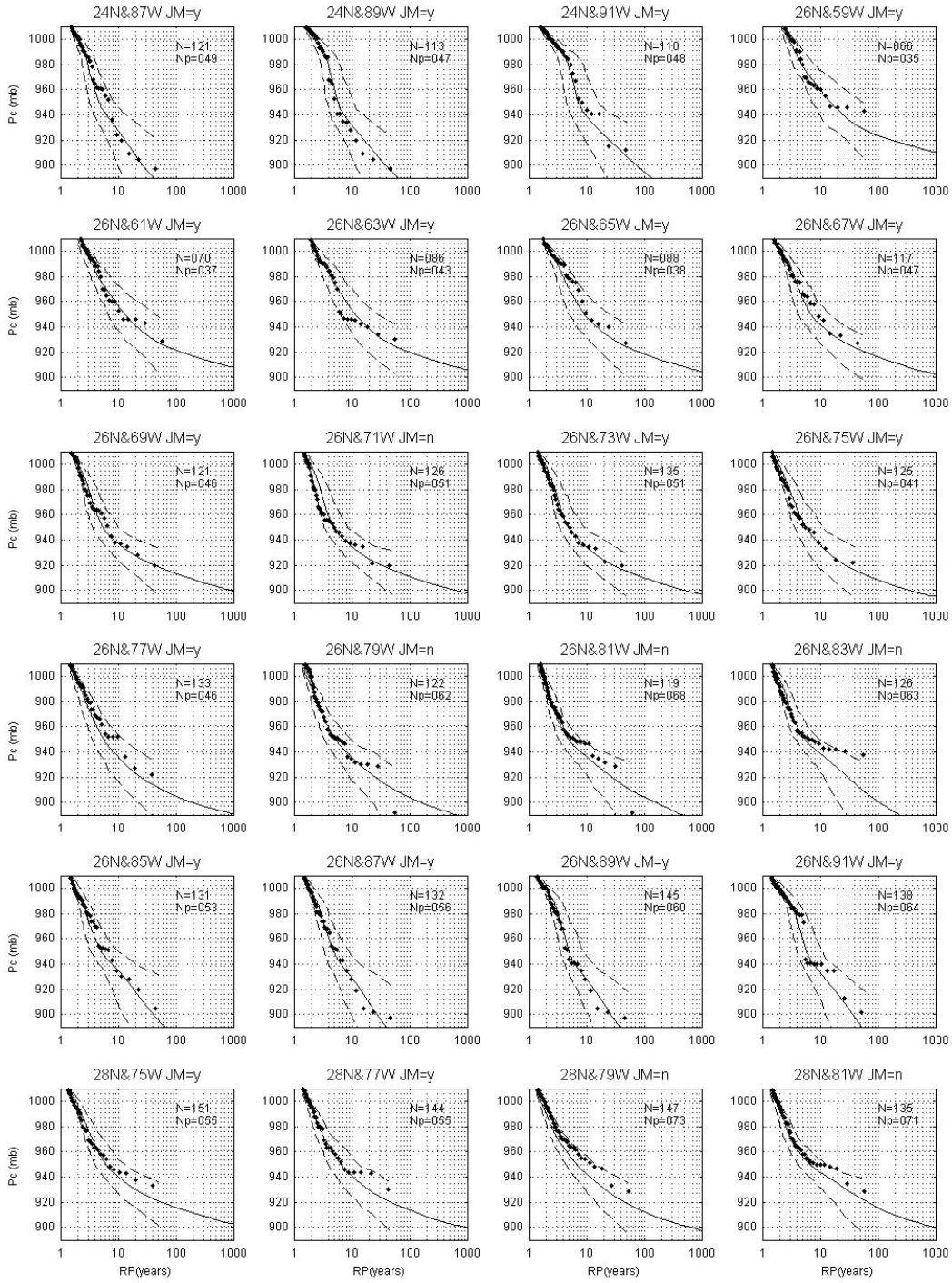

Figure A2. (Continued) Comparison of modelled and observed (1900-2006) central pressures, minimum noted in a 250 km circle around a location, versus return period. Dotted lines show 90% confidence range derived from the modelled empirical distribution. N equals the total number of data points, N_p equals number of points with known central pressure, and JM=n indicates failure of the James & Mason (2005) test.

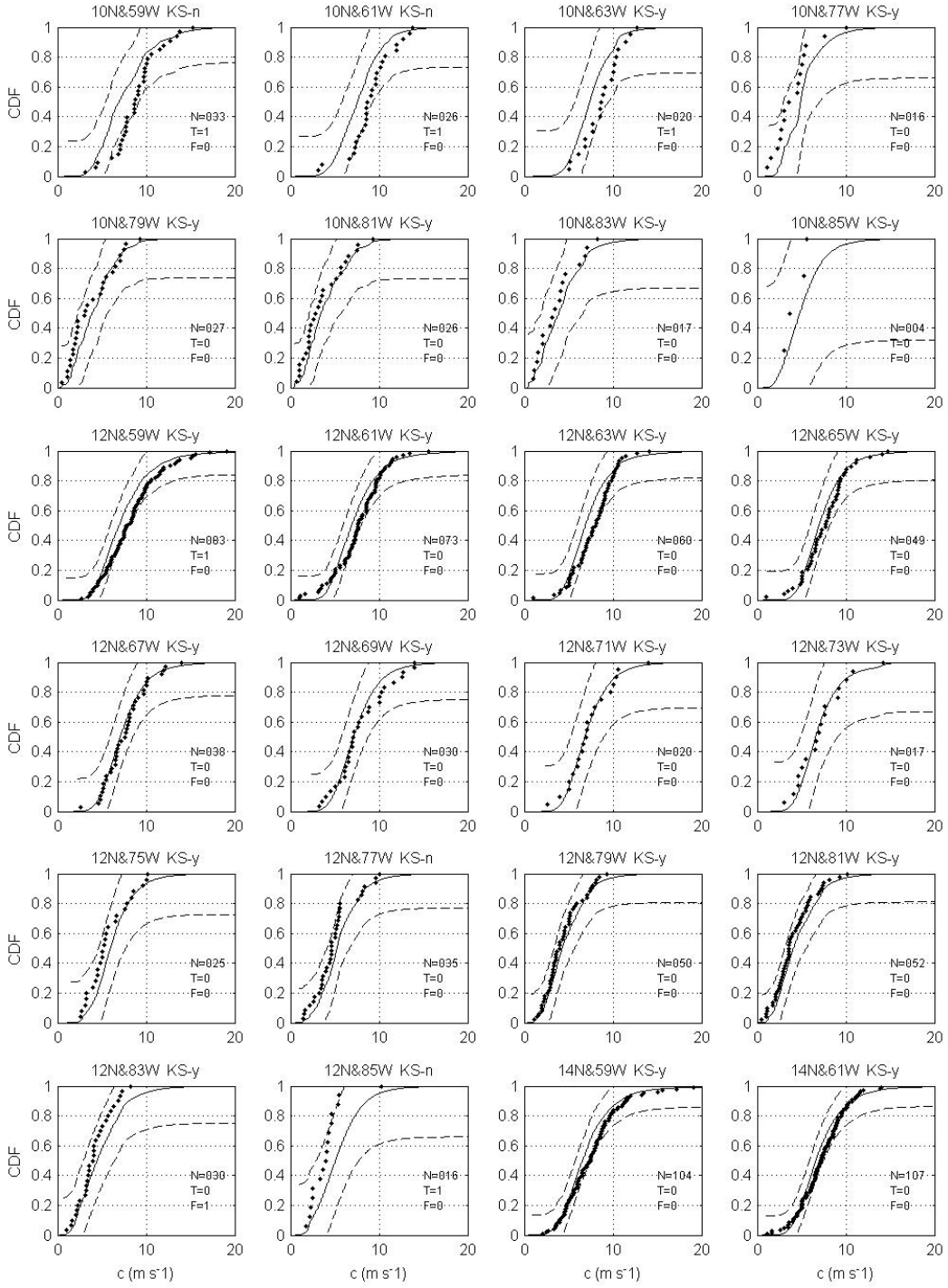

Figure A3. Comparison of modelled and observed (1900-2006) translational speed at specific locations. Dotted lines show 90% confidence range derived from the modelled empirical distribution. N equals the total number of data points, F=1 indicates failure of *F*-test, T=1 indicates failure of *T*-test, and *KS*=n indicates failure of the *KS*-test.

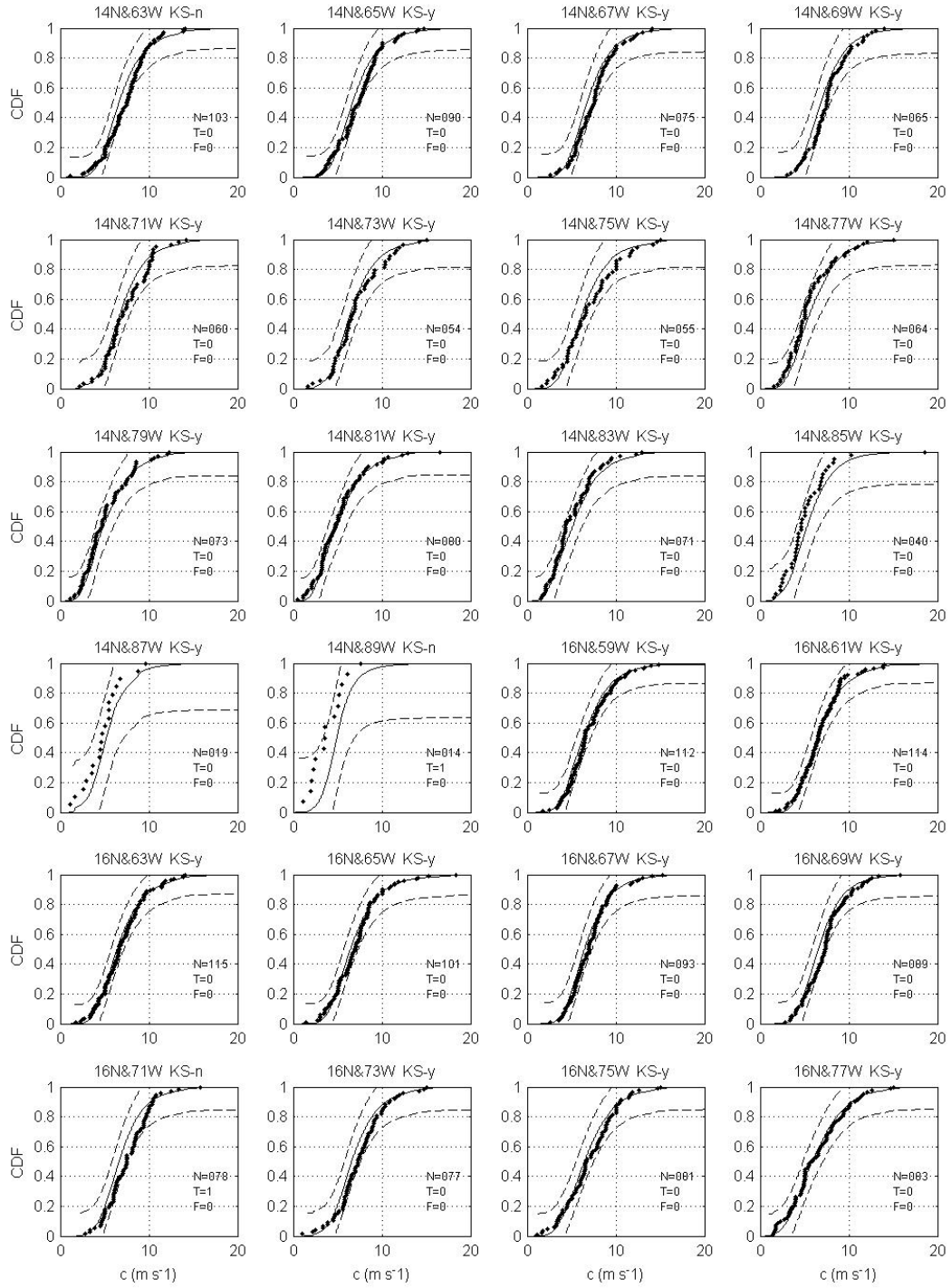

Figure A3. (Continued) Comparison of modelled and observed (1900-2006) translational speed at specific locations. Dotted lines show 90% confidence range derived from the modelled empirical distribution. N equals the total number of data points, F=1 indicates failure of *F*-test, T=1 indicates failure of *T*-test, and *KS*=n indicates failure of the *KS*-test.

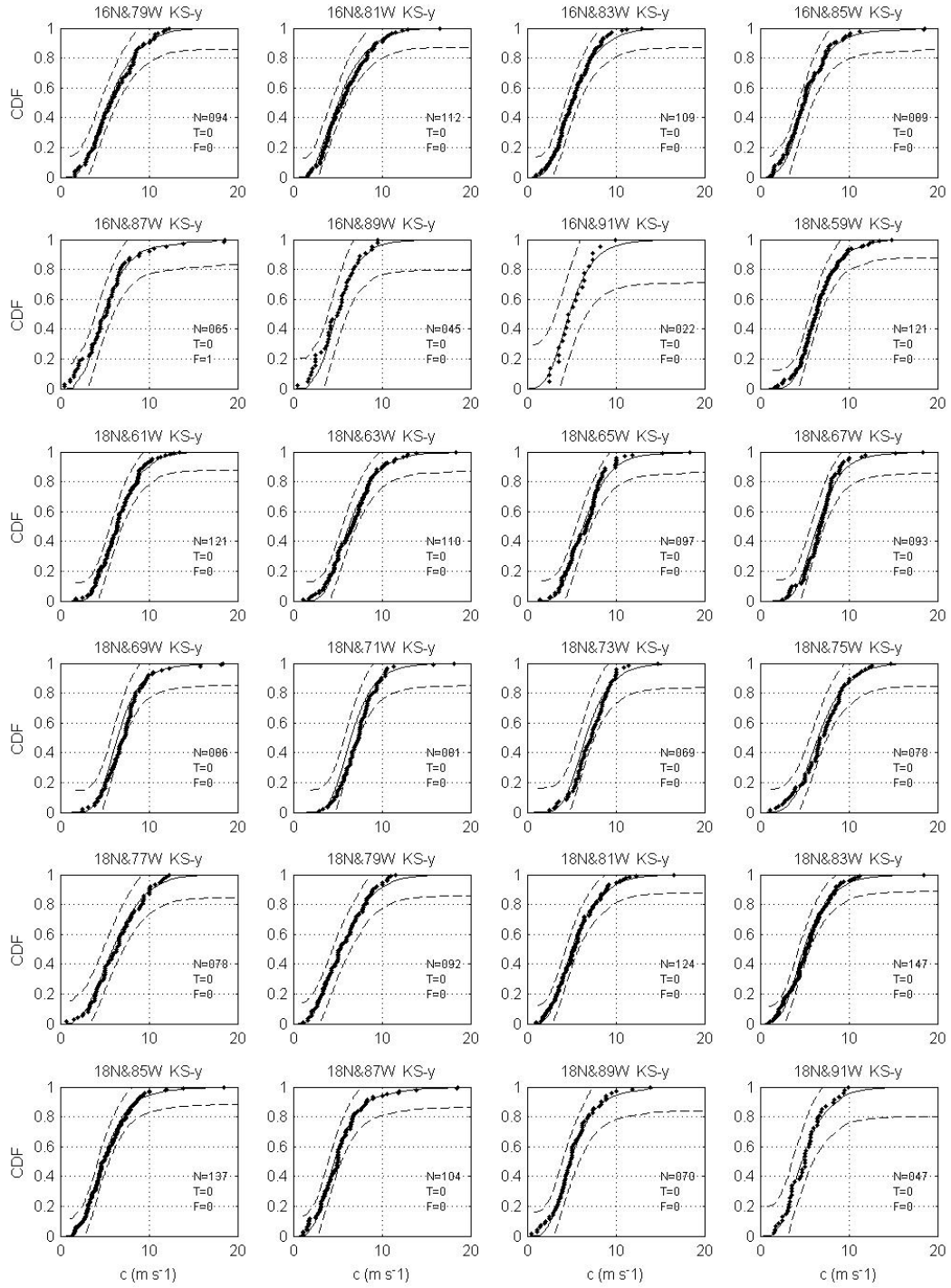

Figure A3. (Continued) Comparison of modelled and observed (1900-2006) translational speed at specific locations. Dotted lines show 90% confidence range derived from the modelled empirical distribution. N equals the total number of data points, F=1 indicates failure of *F*-test, T=1 indicates failure of *T*-test, and *KS*=n indicates failure of the *KS*-test.

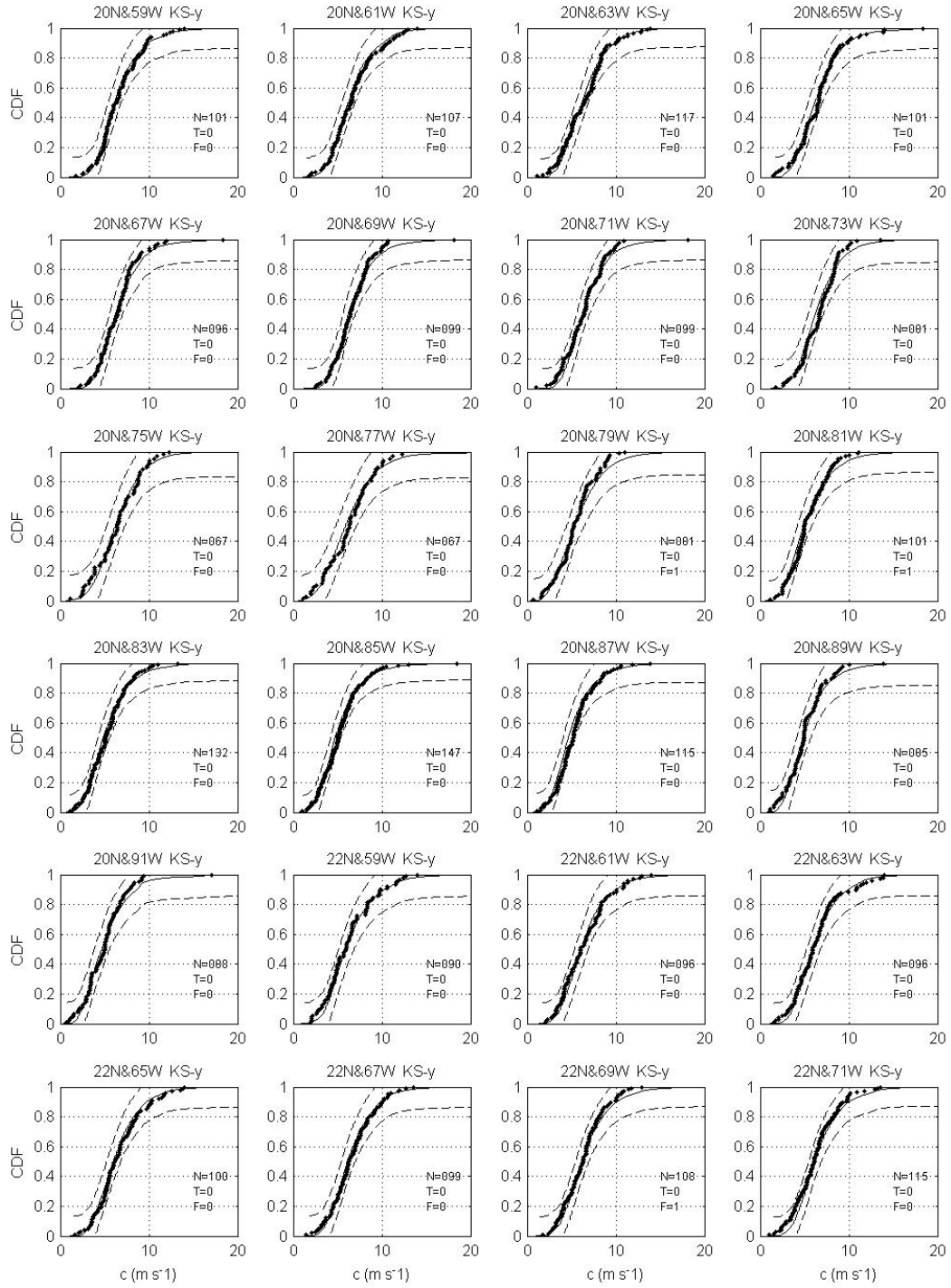

Figure A3. (Continued) Comparison of modelled and observed (1900-2006) translational speed at specific locations. Dotted lines show 90% confidence range derived from the modelled empirical distribution. N equals the total number of data points, F=1 indicates failure of *F*-test, T=1 indicates failure of *T*-test, and *KS*=n indicates failure of the *KS*-test.

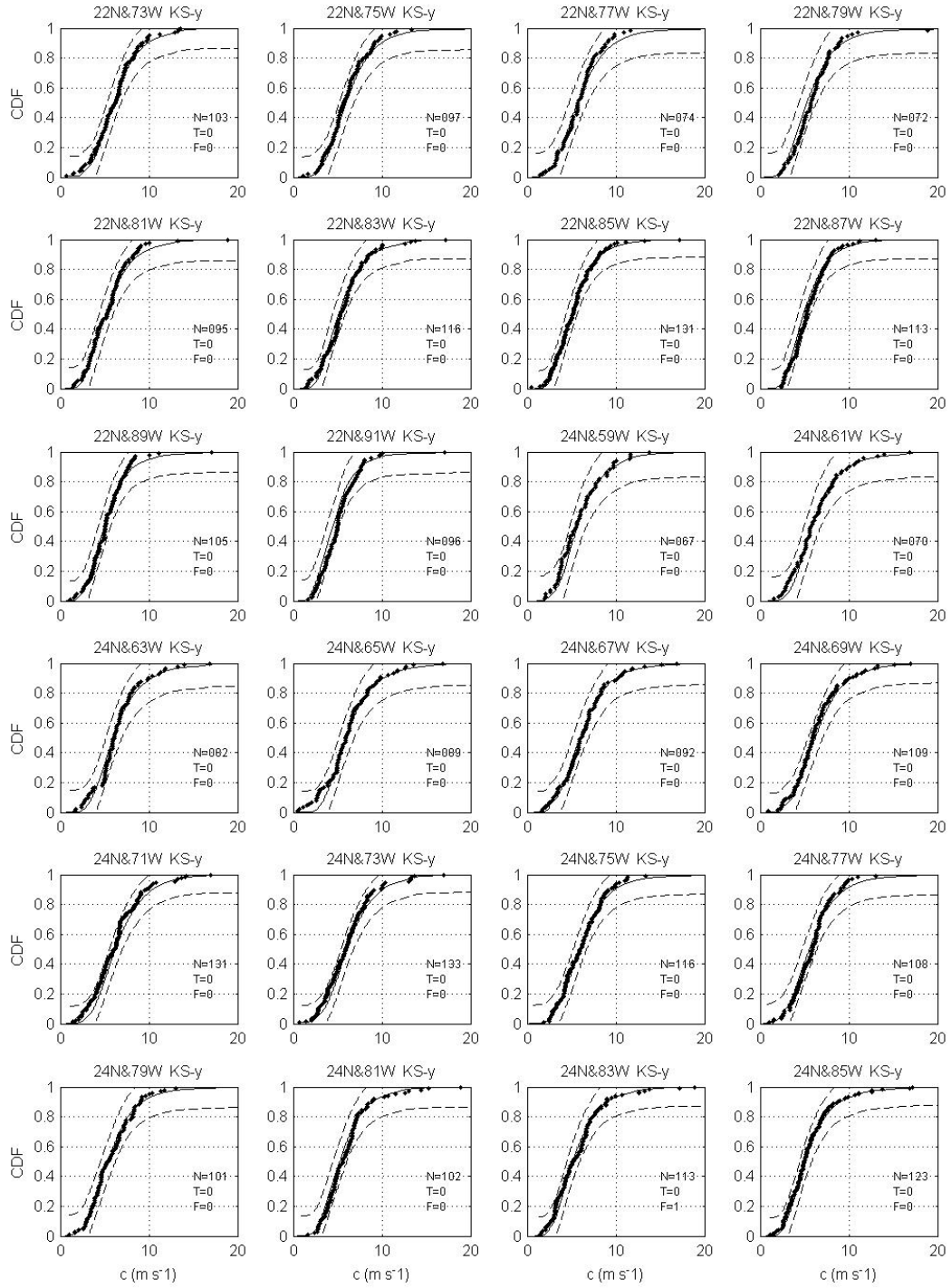

Figure A3. (Continued) Comparison of modelled and observed (1900-2006) translational speed at specific locations. Dotted lines show 90% confidence range derived from the modelled empirical distribution. N equals the total number of data points, F=1 indicates failure of *F*-test, T=1 indicates failure of *T*-test, and *KS*=n indicates failure of the *KS*-test.

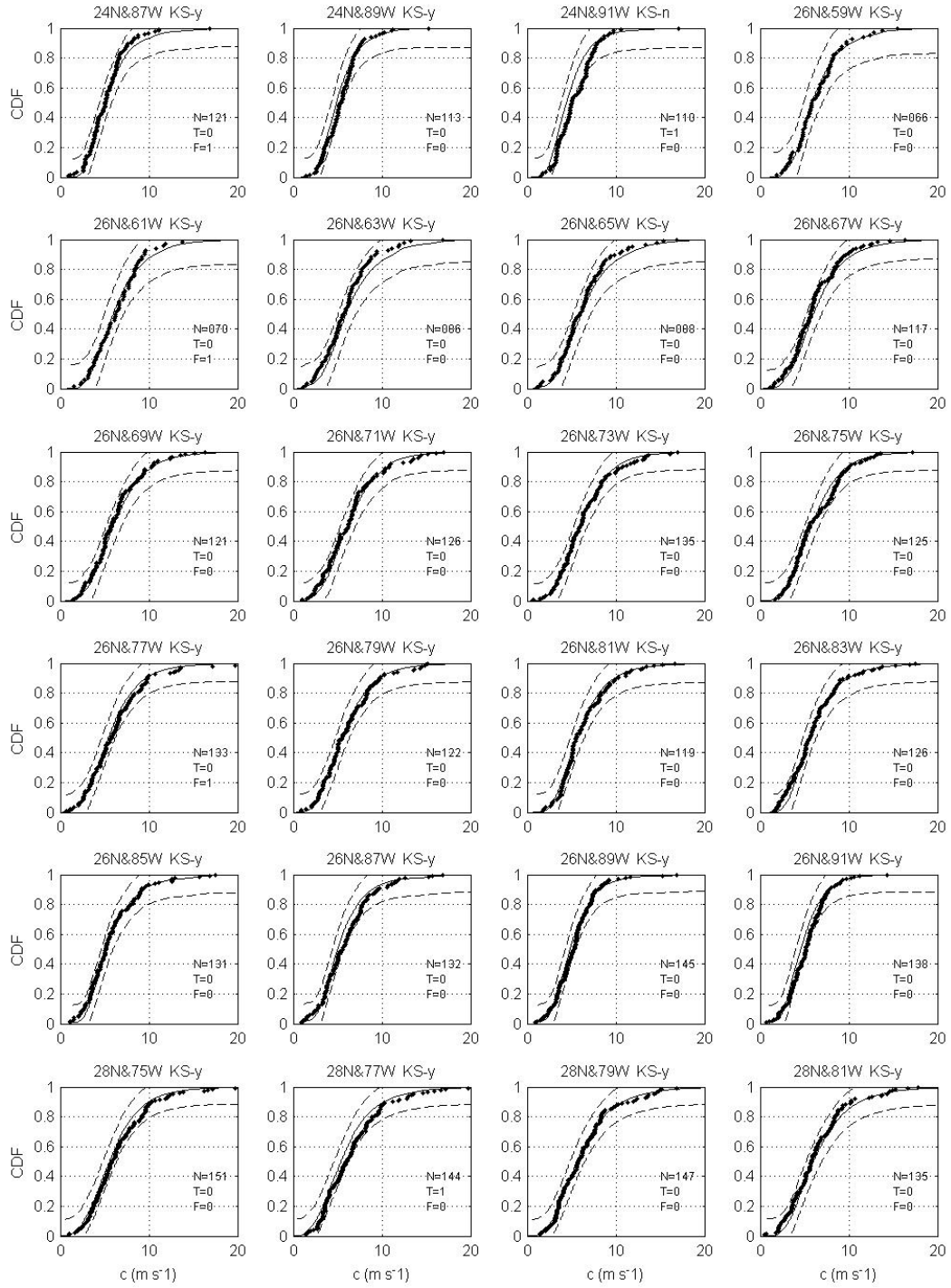

Figure A3. (Continued) Comparison of modelled and observed (1900-2006) translational speed at specific locations. Dotted lines show 90% confidence range derived from the modelled empirical distribution. N equals the total number of data points, F=1 indicates failure of *F*-test, T=1 indicates failure of *T*-test, and *KS*=n indicates failure of the *KS*-test.

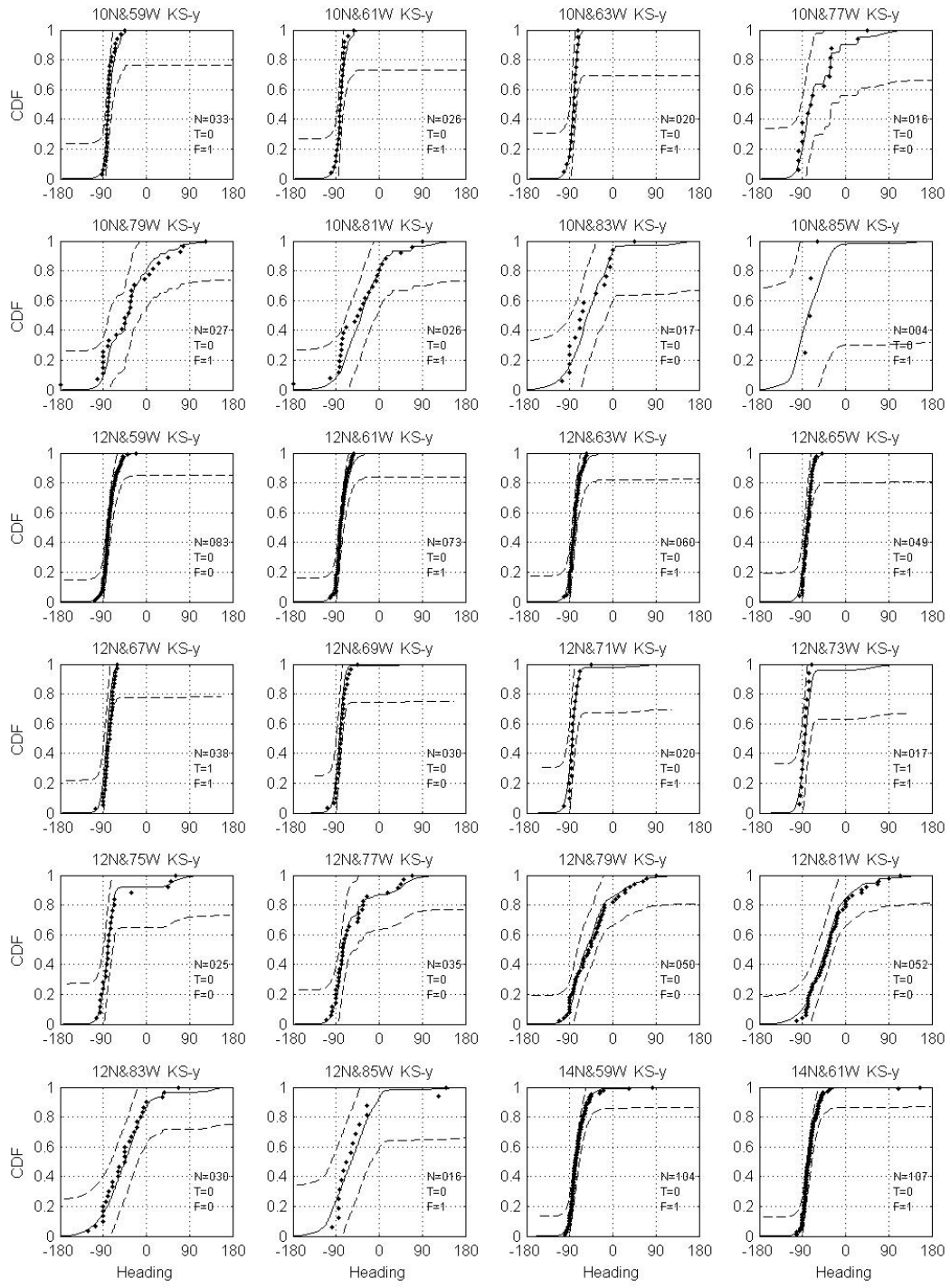

Figure A4. Comparison of modelled and observed (1900-2006) storm heading at specific locations. Dotted lines show 90% confidence range derived from the modelled empirical distribution. N equals the total number of data points, F=1 indicates failure of *F*-test, T=1 indicates failure of *T*-test, and *KS*=n indicates failure of the *KS*-test.

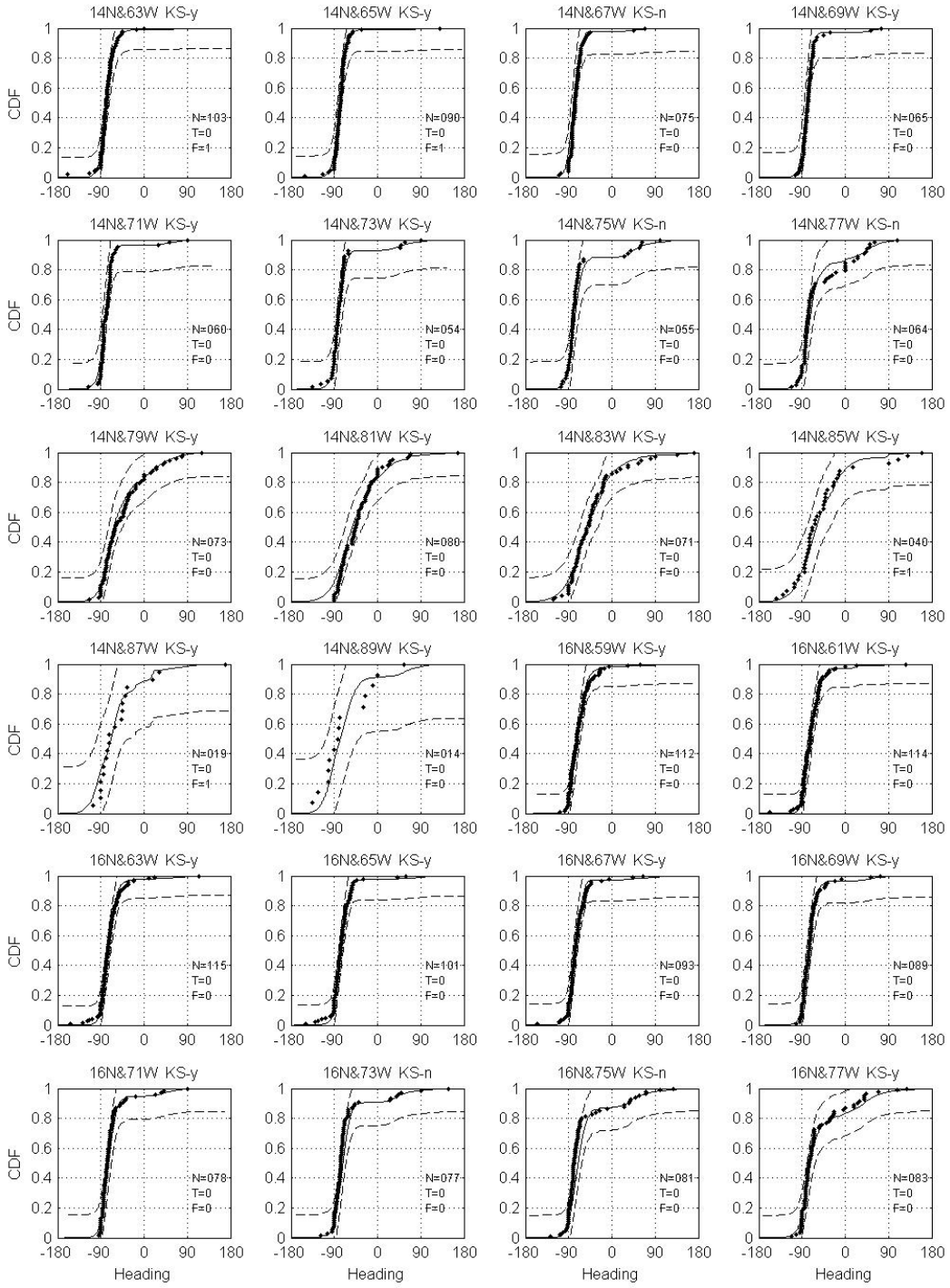

Figure A4. (Continued) Comparison of modelled and observed (1900-2006) storm heading at specific locations. Dotted lines show 90% confidence range derived from the modelled empirical distribution. N equals the total number of data points, F=1 indicates failure of *F*-test, T=1 indicates failure of *T*-test, and *KS*=n indicates failure of the *KS*-test.

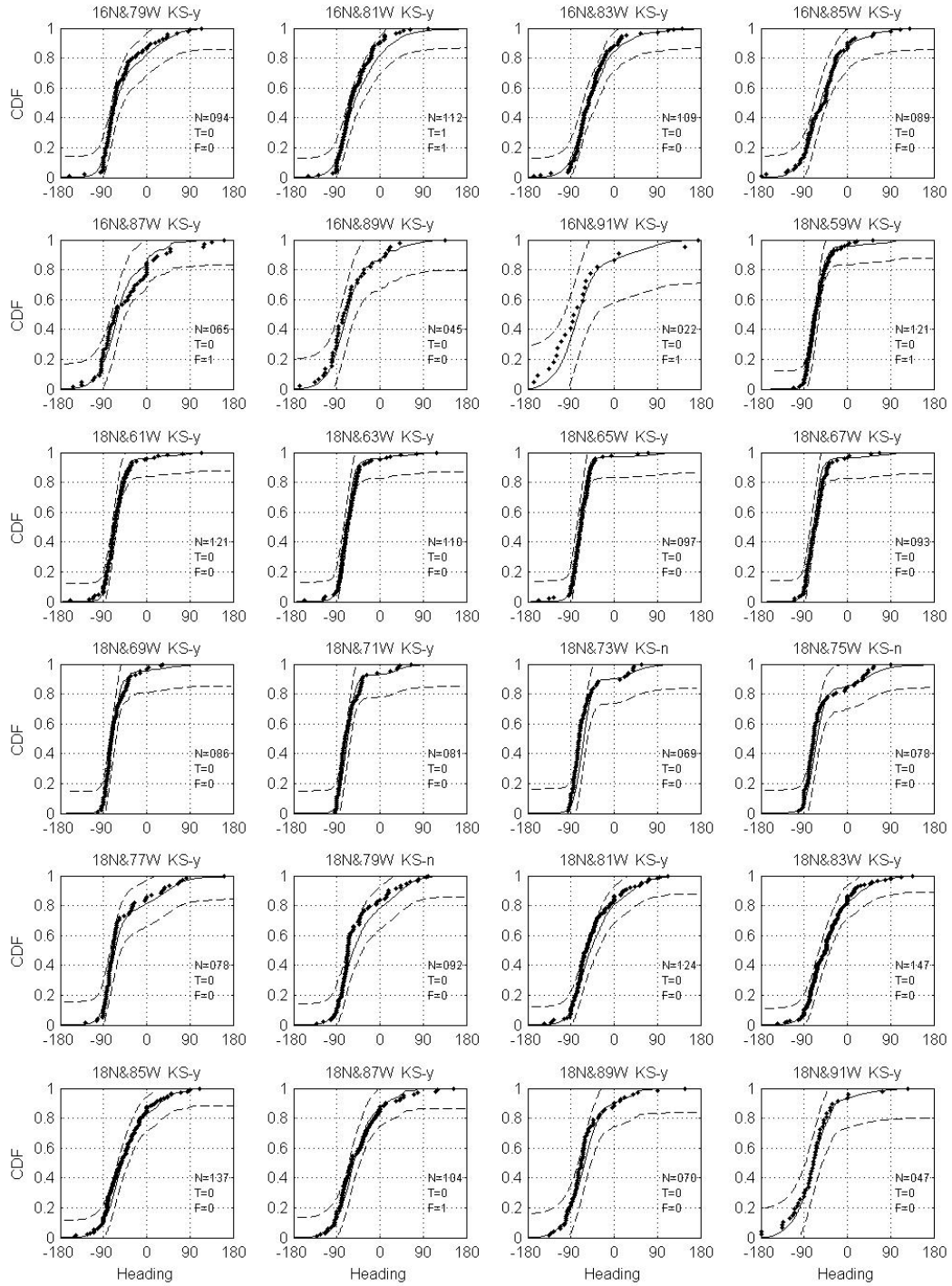

Figure A4. (Continued) Comparison of modelled and observed (1900-2006) storm heading at specific locations. Dotted lines show 90% confidence range derived from the modelled empirical distribution. N equals the total number of data points, F=1 indicates failure of *F*-test, T=1 indicates failure of *T*-test, and *KS*=n indicates failure of the *KS*-test.

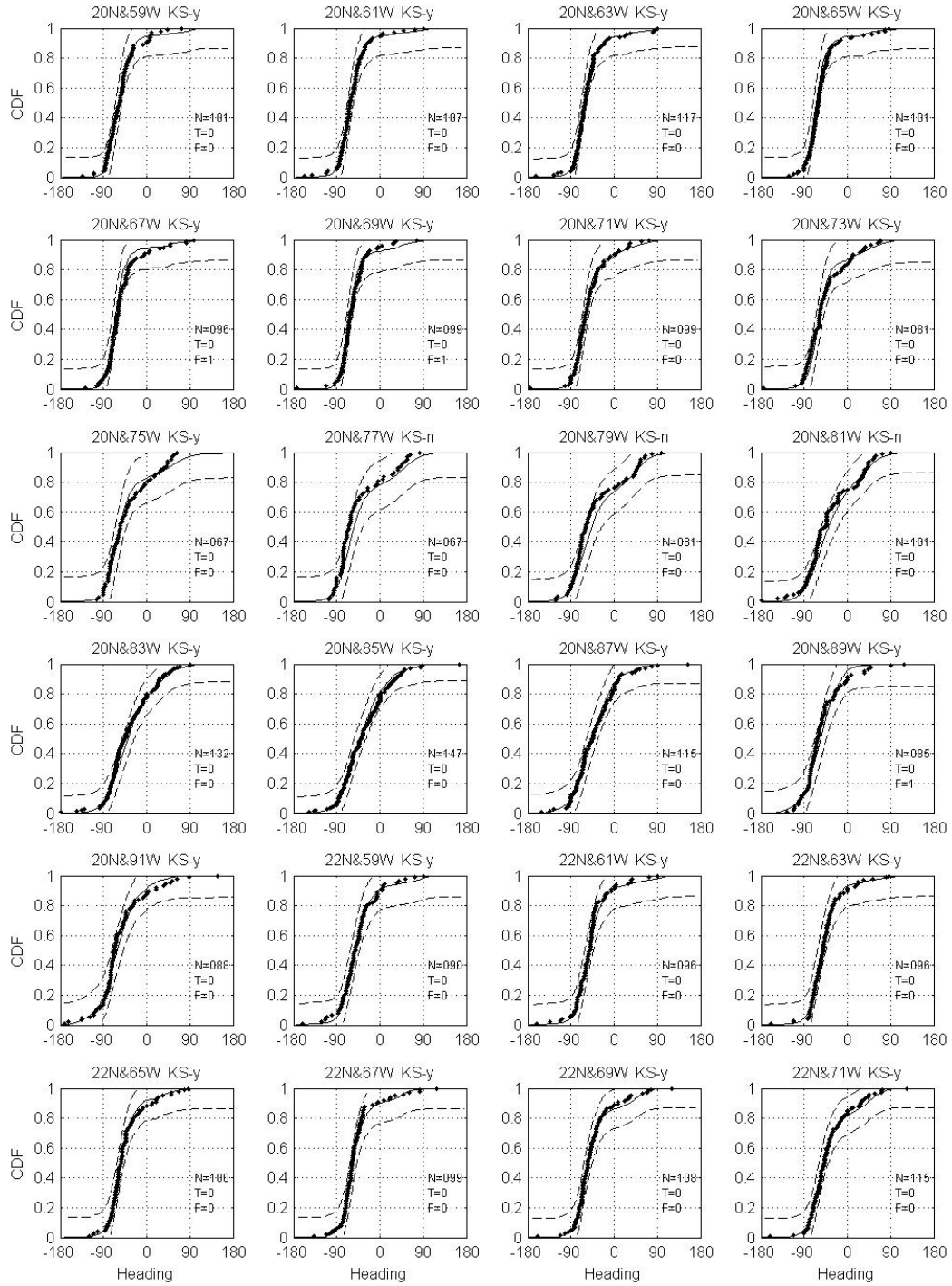

Figure A4. (Continued) Comparison of modelled and observed (1900-2006) storm heading at specific locations. Dotted lines show 90% confidence range derived from the modelled empirical distribution. N equals the total number of data points, F=1 indicates failure of *F*-test, T=1 indicates failure of *T*-test, and *KS*=n indicates failure of the *KS*-test.

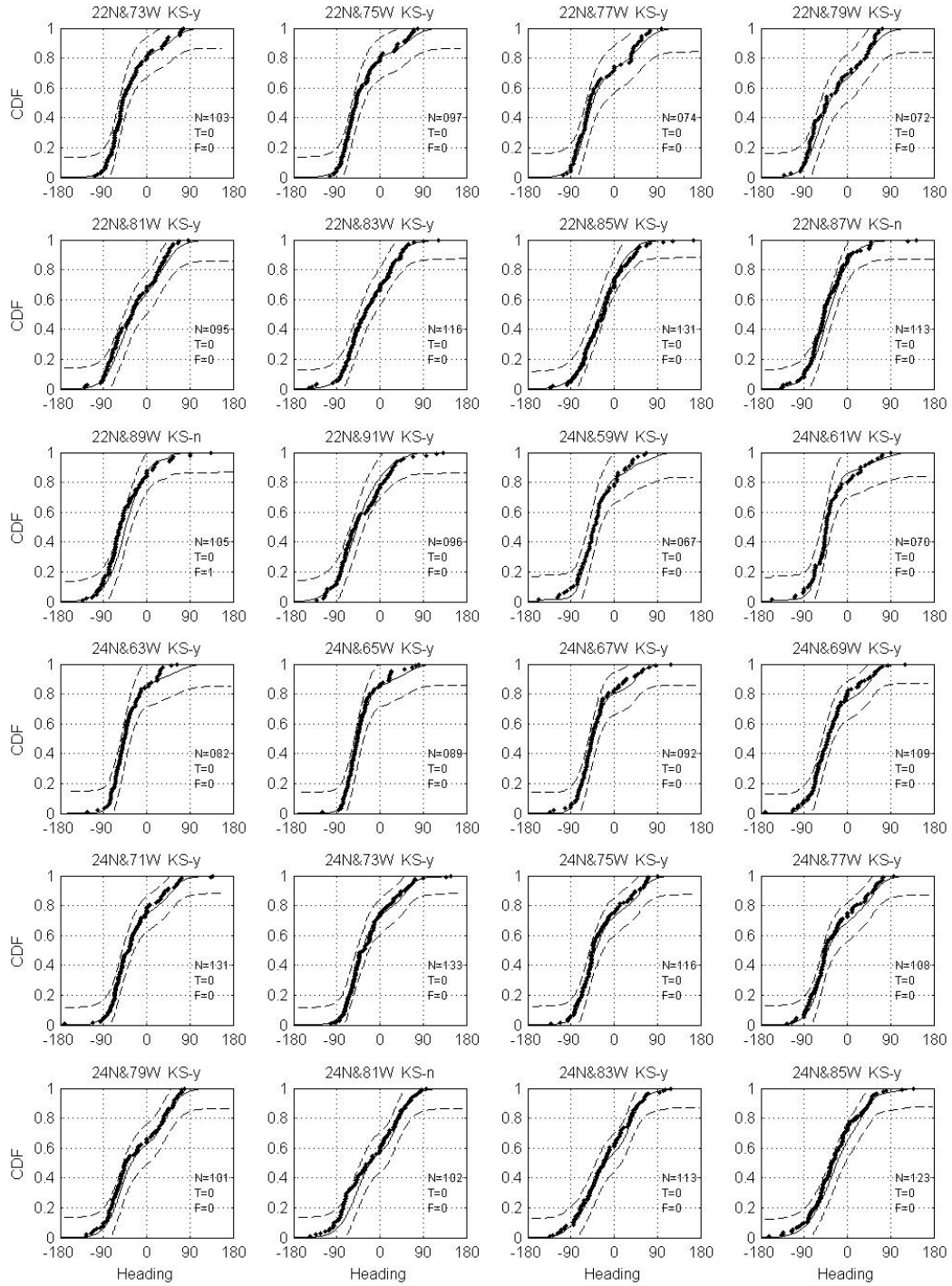

Figure A4. (Continued) Comparison of modelled and observed (1900-2006) storm heading at specific locations. Dotted lines show 90% confidence range derived from the modelled empirical distribution. N equals the total number of data points, F=1 indicates failure of *F*-test, T=1 indicates failure of *T*-test, and *KS*=n indicates failure of the *KS*-test.

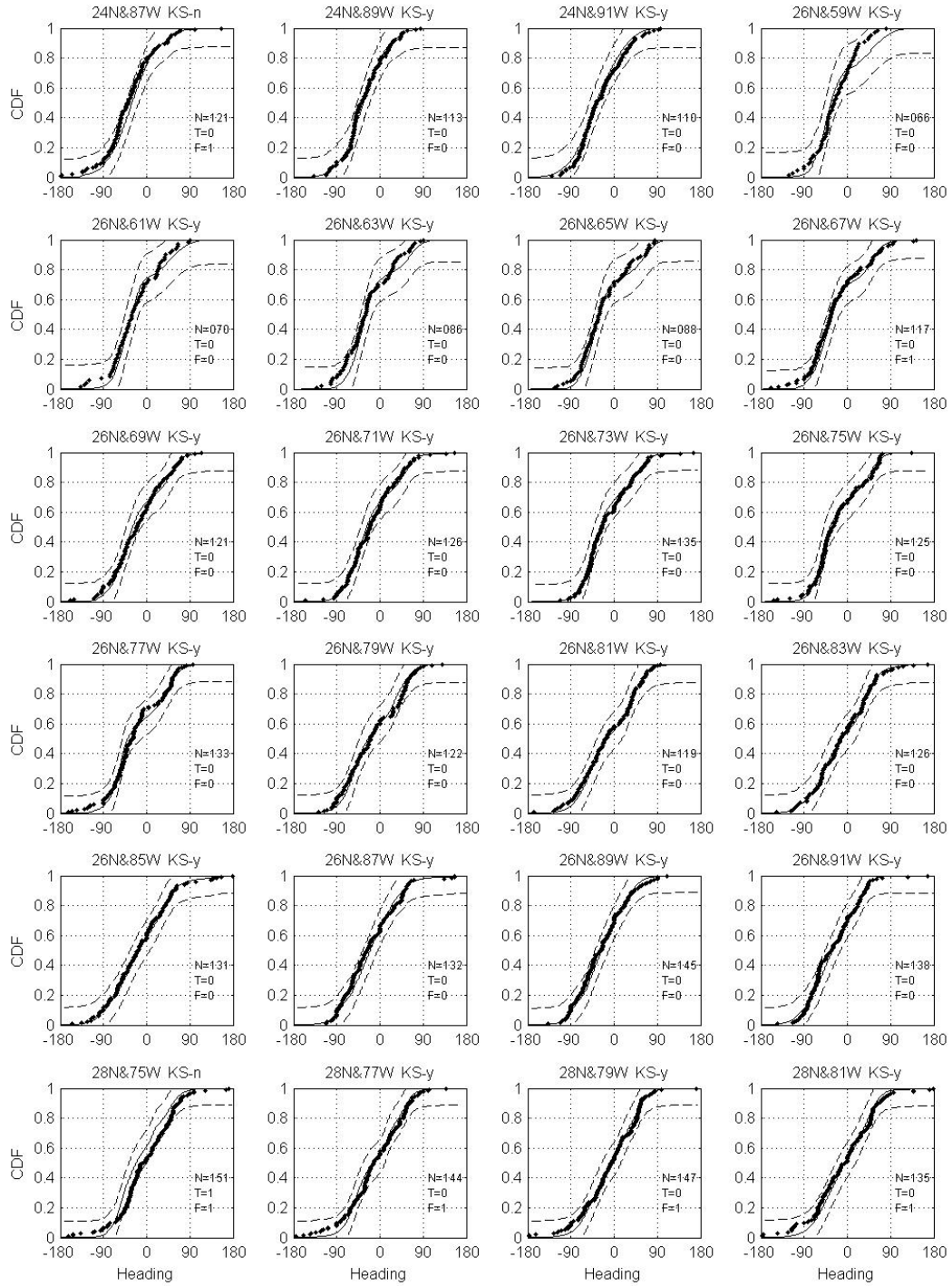

Figure A4. (Continued) Comparison of modelled and observed (1900-2006) storm heading at specific locations. Dotted lines show 90% confidence range derived from the modelled empirical distribution. N equals the total number of data points, F=1 indicates failure of *F*-test, T=1 indicates failure of *T*-test, and *KS*=n indicates failure of the *KS*-test.

Appendix B

Definition of Basic Wind Speeds Used in ASCE 7

The purpose of this appendix is to review the process used by ASCE 7 Wind Load Task Committee (WLTC) in the development of the wind speed map given in ASCE 7-98 and beyond that presents a design wind speed map that is defined by wind speed contours that represents the 500 year return period wind speed divided by the square root of the load factor (i.e. $\sqrt{1.5}$). The goal of the WLTC was to develop a wind speed map that yielded approximately risk consistent designs (for wind resistance) in hurricane and non-hurricane prone regions of the United States. To reach this objective the WLTC developed an approach that, while approximate, resulted in a design wind speed map that incorporated a hurricane importance factor into the specification of the design wind speeds. The approach essentially involved equating the return period associated with exceeding the ultimate wind load in both the non-hurricane and hurricane prone regions of the United States. The methodology allowed for the implied hurricane importance factor to vary with location rather than using a single value as had been used in prior editions of the standard. The approach taken by the WLTC is extended here for the case where the wind load factor is equal to 1.6 rather than 1.5, and is further extended to determine the effective return period associated with the ultimate design of Category III and IV structures (as defined in ASCE 7).

Prior to the introduction of ASCE 7-95, the design wind load equations in ASCE 7 included a multiplicative term in the form of a hurricane importance factor. This hurricane importance factor was introduced to take into account the fact that the tails of the wind speed exceedance probability distributions for hurricane winds are longer than those associated with non-hurricane winds. The hurricane importance factor varied from about 1.05 at the coast and decayed linearly to 1.0 at a distance of 100 miles inland. The hurricane importance factor in ASCE 7 and it predecessor (ANSI A58.1) was applied to the 50-year return period wind speed given in the standard, *not* the resulting velocity pressure. Thus, using the ASCE and ANSI provisions, buildings and structures located near the coast were designed using a wind speed that had a longer return period than those located 100 miles or more inland.

In the development of the wind speed map given in ASCE 7-95, the hurricane importance factor was incorporated directly into the wind speed map (i.e. wind speeds along the hurricane prone at the coast were increased by 5% and wind speeds 100 miles inland were left unchanged, and those in between were adjusted through linear interpolation of the hurricane importance factor).

In the development of the design wind speed map used in ASCE 7-98 the WLTC re-visited the hurricane importance factor that had been in use in the US standards since 1982. The primary reasons for re-visiting the hurricane factor was the recognition that the importance factor likely varied with location along the coast and using a constant value of 1.05 was not appropriate.

The approach taken to develop a varying importance factor began with the premise that the nominal wind load computed using the methods given in ASCE 7, when multiplied by the wind load factor, was representative of an "ultimate" load. Furthermore, it was assumed that the variability of the wind speed dominates the calculation of the wind load factor. The ultimate wind load, *W*, is given as

$$W = C_F (VI_H)^2 W_{LF} \qquad \text{B-1}$$

where C_F is a building/component specific coefficient that includes the effects building height, building geometry, terrain, gust factors, etc., as computed using the procedures outlined in ASCE 7, V is the design wind speed, W_{LF} is the wind load factor, and I_H is the hurricane importance factor.

In order to estimate the value of the hurricane importance factor, I_H, the committee required that the annual probability of exceeding the ultimate wind load in the hurricane and non-hurricane regions of the US should be the same. Note that requiring the annual probability of exceeding the ultimate load in the two areas (hurricane vs. non-hurricane) to be the same does not mean that the annual probabilities of failure are the same. Recalling that the nominal design wind speed in the non-hurricane regions of the United States is associated with a return period of 50 years, the WLTC sought to determine the return period associated with the wind speed producing the "ultimate" load in a representative non-hurricane prone region. As defined in ASCE 7-98, over most of the non-hurricane prone coastline of the United States, the wind speed for any return period can be computed from:

$$V_T / V_{50} = [0.36 + 0.1\ln(12T)] \qquad \text{B-2}$$

where T is the return period in years and, V_T is the T year return period wind speed. In the non-hurricane prone regions of the United States, the ultimate wind load occurs when:

$$W_T = C_F V_T^2 = C_F V_{50}^2 W_{LF} \qquad \text{B-3}$$

thus

$$V_T / V_{50} = [0.36 + 0.1\ln(12T)] = \sqrt{W_{LF}} \qquad \text{B-4}$$

and from B-4, the return period T associated with the ultimate wind speed in the non-hurricane prone portion of the United States is:

$$T = 0.00228 \exp(10\sqrt{W_{LF}}) \qquad \text{B-5}$$

Using the wind load factor of 1.6 as is currently specified in ASCE 7-05, from (B-5) we get T = 709 years.

Figure B-1 presents a comparison of $(V_T/V_{50})^2$ (i.e. a surrogate for the wind load factor) plotted vs. return period for a hurricane (in this case Grand Cayman) and a non-hurricane region. The comparison shows that for T=709 years, the wind loads for a structure located in the hurricane prone region is about twice that of the 50 year return period load. In the non-hurricane prone region this difference is only a factor of 1.6 (i.e. the wind load factor). To ensure the annual probability of exceeding the ultimate wind load for the hurricane and non-hurricane prone regions are the same, a load factor of 2 would have to be applied to the 50 year return period design wind speed for a building designed at the hurricane prone location, whereas a load factor of 1.6 is applied to the non-hurricane wind load.

Alternately, from Equations B-1 and B-3, a hurricane importance can be defined as

$$I_H = \sqrt{2/1.6} = 1.12 \qquad \text{B-6}$$

Or more generally,

$$I_H = (V_{709}/V_{50})/\sqrt{W_{LF}} \qquad \text{B-7}$$

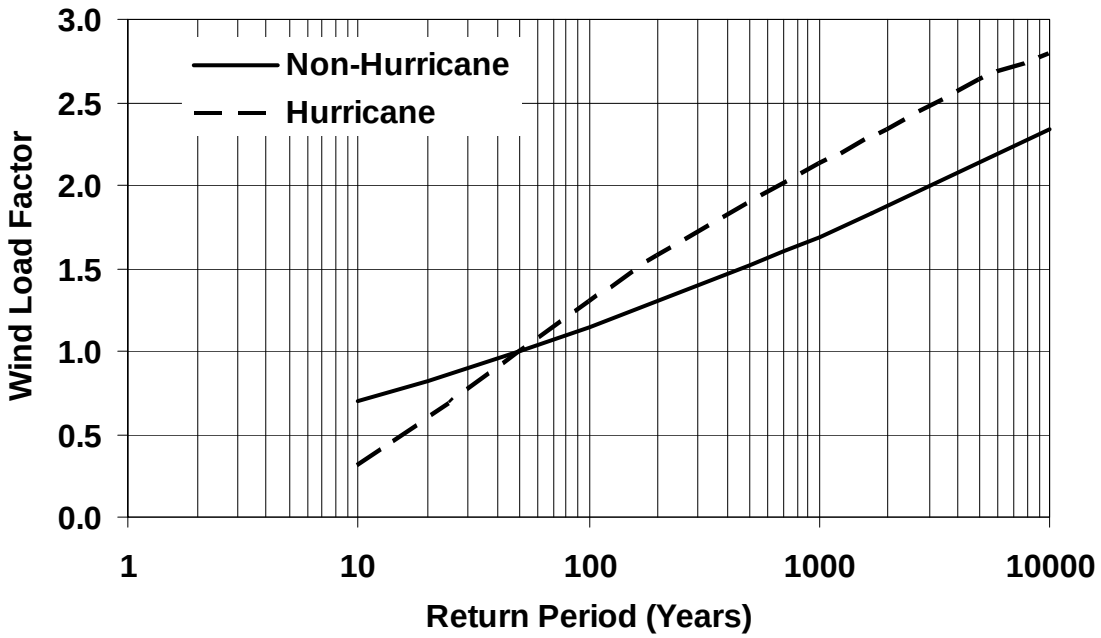

Figure B-1 Wind load factor $(V_T/V_{50})^2$ for Hurricane and Non-Hurricane Wind Speeds plotted vs. return period.

Thus when the 50 year return period wind speed in the hurricane prone region is multiplied by the hurricane importance factor, the annual probability that the ultimate load is exceeded in either location is about the same.

Instead of producing maps of hurricane importance factors to be applied to the nominal 50-year return period wind speed, a design wind speed can be defined as:

$$V_{design} = V_{709} / \sqrt{W_{LF}} \approx V_{700} / \sqrt{W_{LF}} \qquad \text{B-8}$$

Using a wind speed defined as in Equation B-8 eliminates the need to develop a map for both the 50-year return period wind speed and the importance factor. If a basic (design) wind speed associated with a 50 year return period was used in the Caribbean, in order to be consistent with the intent of the ASCE 7 standards, a load factor defined as $(V_{700}/V_{50})^2$ would be used in place of a constant value of 1.6. Figure B-2 presents contours of $(V_{700}/V_{50})^2$ showing the variation of the effective wind load factor over the Caribbean basin, varying from about 1.75 around Puerto Rico to in excess of 6 near Trinidad and Tobago. The very large ratios in the southern portion of the Caribbean occur because of the large number of years where the locations do not experience any hurricanes, and as a result the 50 year return period wind speeds are very low, but these locations experience strong winds from hurricanes associated with rare events.

Note that when the wind speed maps were being developed for ASCE 7-98, the wind load factor at the time was equal to 1.53, which the wind load task committee rounded down to 1.5 and computed an ultimate load return period of 475 years, which subsequently rounded up to 500 years. The final wind speed map used in ASCE 7-98 was developed using $V_{design} = V_{500} / \sqrt{1.5}$. During the same time period when the wind load map was being developed, the ASCE 7 committee examining load factors increased the load factor from a value of 1.53 to 1.6. Thus when ASCE 7-98 was published there was a disconnection between the load factor used to develop the map and the load factor used in the wind loading equations.

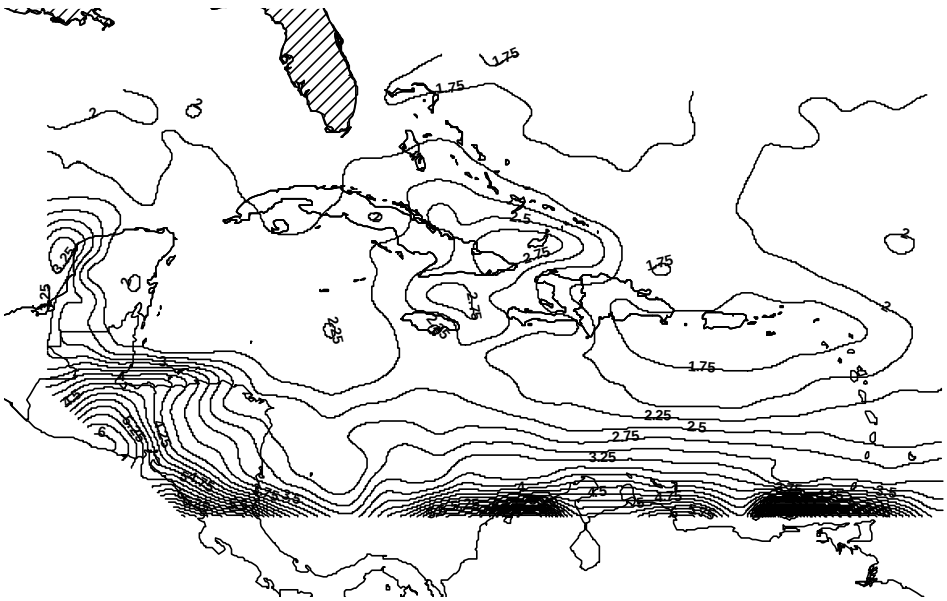

Figure B-2 Contour plots of $(V_{700}/V_{50})^2$

As indicated above, when the correct load factor of 1.6 is used, a design wind speed defined as $V_{design} = V_{700} / \sqrt{1.6}$ is appropriate. This design wind speed is equivalent to designing a structure using the 700 year return period wind speed and a load factor of unity.

The importance factor used in ASCE 7 for the computation of wind loads for the design of category III and IV structures is defined so that the nominal 50-year return period non-hurricane wind speed is increased to be representative of a 100-year return period value. This importance factor *is not* the hurricane importance factor, $I_{H,}$ but rather a factor used to increase the wind loads based on an occupancy classification. The importance factor is applied to the design of all category III and IV buildings whether or not they are located in a hurricane prone region. Following the approach used above to estimate the resulting ultimate load return period associated with the 100 year design wind speed in the non-hurricane prone regions we find that:

$$T = 0.00228 \exp[10(V_{100} / V_{50})\sqrt{W_{LF}}] \qquad \text{B-9}$$

where for V_{100} / V_{50} computed from B-4 and W_{LF} = 1.6, we find that T=1,697 years. In the development of Equation B-9, the term $(V_{100} / V_{50})\sqrt{W_{LF}}$ replaces the $\sqrt{W_{LF}}$ used in Equation B-5, effectively resulting in a higher load factor for category III and IV structures equal to $W_{LF}(V_{100} / V_{50})^2$. Thus for Category III and IV structures, a design wind speed of $V_{1700} / \sqrt{1.6}$ is appropriate.

In the versions of ASCE 7 since 1993 (i.e., ASCE 7-95 and beyond), the importance factor has been applied to the velocity pressure, *not*, the wind velocity as was the case in prior editions. The design pressure in ASCE 7-95 and later is

$$q_z = 0.00256 K_z K_{zt} K_d V^2 I \qquad \text{B-10}$$

where the importance factor I is equal to 1.15 for category III and IV structures. For consistency in the hurricane prone regions, the importance factor should be defined as:

$$I = (V_{1700} / V_{700})^2 \qquad \text{B-11}$$

Figure B-3 presents contour plots of $I = (V_{1700} / V_{700})^2$ where a large gradient of I from north to south is evident, but over most of the region, I, is consistent with the 1.15 value given in ASCE 7. In the case of the Category II buildings where a 700 year return period wind speed represents an ultimate design wind speed for these Category II buildings, we find that for Category III and IV buildings a 1,700 year return period wind speed is representative of the ultimate wind load. Both approaches inherently include the variation in the hurricane importance factor in hurricane prone regions, but are tied back to a wind load factor equal to 1.6 as applied to the non-hurricane prone region of the United States.

Figure B-3 Contour plots of importance factor for ASCE category III and IV structures defined by $I=(V_{1700}/V_{700})^2$